Advances in Nano Research, *Vol. 13, No.4 (2022) 351-368*
https://doi.org/10.12989/anr.2022.13.4.351

An efficient C^1 beam element via multi-scale material adaptable shape function

A. M. El-Ashmawy*[1] and Yuanming Xu[2,3a]

[1]*Department of Aircraft Mechanics*, *Military Technical College*, *Cairo*, *Egypt*
[2]*School of Aeronautic Science and Engineering*, *Beihang University*, *Beijing*, *100191*, *China*
[3]*Beijing Advanced Discipline Center for Unmanned Aircraft System*, *Beijing*, *China*

(*Received December 16, 2020, Revised May 23, 2022, Accepted July 3, 2022*)

Abstract. Recently, promising structural technologies like multi-function, ultra-load bearing capacity and tailored structures have been put up for discussions. Finite Element (FE) modelling is probably the best-known option capable of treating these superior properties and multi-domain behavior structures. However, advanced materials such as Functionally Graded Material (FGM) and nanocomposites suffer from problems resulting from variable material properties, reinforcement aggregation and mesh generation. Motivated by these factors, this research proposes a unified shape function for FGM, nanocomposites, graded nanocomposites, in addition to traditional isotropic and orthotropic structural materials. It depends not only on element length but also on the beam's material properties and geometric characteristics. The systematic mathematical theory and FE formulations are based on the Timoshenko beam theory for beam structure. Furthermore, the introduced element achieves C1 degree of continuity. The model is proved to be convergent and free-off shear locking. Moreover, numerical results for static and free vibration analysis support the model accuracy and capabilities by validation with different references. The proposed technique overcomes the issue of continuous properties modelling of these promising materials without discarding older ones. Therefore, introduced benchmark improvements on the FE old concept could be extended to help the development of new software features to confront the rapid progress of structural materials.

Keywords: finite element modeling; functionally graded material; functionally graded nanocomposites beams; isotropic; nanocomposites; orthotropic; timoshenko beam element

1. Introduction

Advanced structure requirements aim to create a multi-role, high-performance, ultra-load resistance, durable, environmentally safe and low-cost structures. Moreover, revolutionary progress on production techniques such as 3D printing and additive manufacturing made complex shapes and nontraditional parts easy to fabricate (Li *et al*. 2019). Therefore, systems designers feel freer and optimistic about their optimized shapes and components. These factors put more pressure on structural engineers and increase challenges for them. Furthermore, they have to deal with these goals like (1) identifying and proposing the advanced materials, (2) theoretical modeling and analysis of structural parts of these materials and (3) verifying the performance of them in view of structural integrity, experimentally. In the historical view, materials development undergoes by starting using natural materials such as wood. Mining materials like aluminum and steel and nowadays, the laboratory developed materials such as piezoelectric, shape memory alloys and nanomaterials (Bogue 2014). These materials complex the structural elements into smart structures, FGM parts, or nanostructures. These evolutionary variations give particular interest in structural modeling and analysis of these significantly sophisticated shapes with the progressing of advanced materials.

Beam structural modeling and analysis are considered in this study based on the Timoshenko beam theory (TBT) or the first-order shear deformation theory. It assumed that straight lines perpendicular to the mid-plane before bending remain straight but no longer stay perpendicular. However, the transverse shear stress concerning the thickness coordinate is considered constant, TBT represented pivotal theory in beam modeling and analysis. The second-order shear deformation theory further relaxes the kinematic hypothesis by removing the straightness assumption, i.e., the straight normal to the middle plane before deformation may become cubic curves after deformation. The third-order shear deformation theory, which assumed parabolic distribution of the transverse shear stress and strain concerning the thickness coordinate, was proposed for beams with rectangular cross-sections. Also, zero transverse shear stress condition of the upper and lower surface of the cross-section is satisfied without utilizing the shear correction factor. Higher order shear deformation theories loosen up hypothesis and converge to the real exact value through more complex explanation for shear and coupling behavior. There are many researchers studied application of these different theories on nanocomposite materials such as (Ebrahimi and Dabbagh 2018a, b, c, 2020b, d, Ebrahimi *et al*. 2019b, 2021c, b, Yarali *et al*. 2020).

*Corresponding author, Ph.D.,
E-mail: abdelmaged46@mtc.edu.eg;
elashmawy@buaa.edu.cn
[a]Professor

ISSN: 2287-237X (Print), 2287-2388 (Online)

FE depends on a simple solution assumption where the convergence rate increases with the number of elements and mesh size. Therefore, the obtained results before convergence are rough and cannot represent accurately, underestimate, the mechanical properties of the studied domain. Accordingly, it converges always at the upper bound. On the other hand, method such as Differential Quadratic Method (DQM) obtained a suitable balance between accuracy and complexity. So, the convergence cannot be predicted on the upper or lower bound precisely. Therefore, FE is a method for finding approximate numerical solutions to field problems. Moreover, FE method has many advantages as it applied to any field problem with boundary conditions, loading types and material properties that are not restricted (Cook *et al*. 2007). On the other hand, the analytical solution has minimal capabilities for all these parameters. The development of FE techniques continued to increase reliability, applicability and calculations time reduction, where recent researches studied advanced approaches as (Sevilla *et al*. 2011, Baiges *et al*. 2020). Shape function represents the main characteristic of any FE solution. It was extensively investigated in many kinds of research such as (Iwai and Kobayashi 2003, Bazoune *et al*. 2003, Ping 2005, Takahashi 2006, Li *et al*. 2013, Panchore *et al*. 2015, Tudjono *et al*. 2017).

The isotropic materials are the broadest used materials in structural engineering. Many types of research investigated isotropic beam structures modeling and analysis concerning the FE method. It was historically well-developed with time, for example and not as a limitation (Eisenberger 2003, Elshafei 2013, Sahin *et al*. 2019, Zhou *et al*. 2019, Feng and Wu 2020). Eisenberger (1994) was the first one who introduced the method for direct derivation of exact shape function from differential equations. This research also presented super-convergence FE beam modeling using TBT. Reddy (1997) investigated and defined free-off shear locking deformable beams FE modeling. After-by, the global needs for stiffer material and lower specific density increased. That is why orthotropic materials such as fiber-composites occupied an essential place at the moment of its discovery. It is extensively used in many applications like aerospace engineering and studied in many kinds of research, such as (Minghini *et al*. 2007, Kennedy *et al*. 2011, Hou and He 2018, Mansouri *et al*. 2020, Lezgy-Nazargah 2020). The lamination concept and changing properties in the different directions pushed research to create advanced methods in modeling. However, it kept the same shape function with the old concept depending only on the element length. Moreover, it has drawbacks, such as stress concentration between layers and delamination problems.

In the modern era, development continues. The properties are changed from being constant in each direction with different values to being more sophisticated as the corresponding coordinate function. This target can be achieved by combining two or more materials in a micro-scale with different percentages along with specific coordinates such as thickness direction, producing the so-called FGM (Suresh and Mortensen 1998). This continuous changing of properties' main target is to eliminate stress concentration between layers on composite material. FGM has a particular privilege over other materials from a thermal resistance point of view (Reddy and Chin 1998). Therefore, it is nominated to be used in the heat-resistant aircraft engine parts and space shuttle shielding (Li and Han 2018). This progress made an FE modeling challenge. Infinitesimal layers simulation is the only way to approach grading properties in a specific direction and to approximate the continuity, which is not achieved. Therefore, the old shape function concept needs to develop because it depends only on element length. Chakraborty *et al*. (2003) were one of the pioneers who introduced the concept of new shape function depending on material properties to analyze FG beams. The efficiency and accuracy of 1-D elements in FGM beams analysis were proved after comparison with 1-, 2- and 3-D published results by Filippi *et al*. (2015). This research introduced 1-D Carrera Unified Formulation to analyze FGM beams statically. Moreover, Frikha *et al*. (2016) used a mixed high order C0 element to analyze FGM beams. Static and vibration analysis was investigated recently by Katili *et al*. (2020), Khan *et al*. (2020) to discover the whole FGM structure aspects and unobserved behavior. In the last decades, FGM structures were enormously studied, such as (El-Ashmawy *et al*. 2016a, b, Rajasekaran and Khaniki 2018, Berghouti *et al*. 2019, Haskul 2020, Huang and Ouyang 2020, Zhou *et al*. 2020, Sinha and Kumar 2020).

Nanocomposites are introduced as an alternative material in structural engineering. Carbon Nanotubes Reinforced Composites (CNTRC) and graphene are examples of nanocomposite reinforcements. It promises exceptional strength and stiffness with the lowest specific weight (Thostenson *et al*. 2001). A combination of nano-technology and FG concept is introduced to produce advanced structures such as Functionally-graded Carbon Nanotubes Reinforced Composites (FG-CNTRC) and FG graphene nanocomposite. This development requires more modification on the shape function concept to analyze structures and fill the gap between macro and micro-scale structures. Yas and Heshmati (2012) investigated FG-CNTRC beams dynamic analysis with randomly oriented CNT and subjected to moving loads. Also, Heshmati and Yas (2013) proposed the Eshelby-Mori-Tanaka approach to study the free-vibration of FG-CNTRC beams. FG-CNTRC beams were represented to be laminated with different distributions by Vo-Duy *et al*. (2019) through free-vibration analysis. Recently, CNTRC and FG-CNTRC structure modeling and analysis were extensively represented in (Ke *et al*. 2013, Aydogdu 2014, Wu *et al*. 2016, Ebrahimi and Habibi 2017, Ranjbar and Feli 2018, Wu *et al*. 2019, Emdadi *et al*. 2019, Hocaoğlu and Karagülle 2020, Talò *et al*. 2020, Selvaraj and Ramamoorthy 2020, El-Ashmawy and Xu 2020, Tayeb *et al*. 2020, Soni *et al*. 2020, Zerrouki *et al*. 2020, El-Ashmawy and Xu 2021, El-Ashmawy *et al*. 2021). Moreover, graphene nanocomposite and its grading were also investigated on many published pieces of research as (Liu *et al*. 2020, Barati and Shahverdi 2020, Wang *et al*. 2020, Mojiri and Salami 2020). Also, wave propagation/ dispersion of nanostructures and FG-nanostructures were extensively studied in (Ebrahimi and Dabbagh 2019a, c, d,

Ebrahimi *et al*. 2018, 2019a, c, d, 2021c). Moreover, multi-scale nanocomposites were investigated in (Ebrahimi and Dabbagh 2019b, 2021, Ebrahimi *et al*. 2021a, e, Dabbagh *et al*. 2021). However, many investigations have been performed. Nanocomposites still suffered from severe problems in production techniques such as aggregation and insufficient bonding. A few researches investigated the negative effects of agglomeration and waviness phenomena on the material properties of the nanocomposite such as (Ebrahimi and Dabbagh 2019d, 2020a, c, Farzad Ebrahimi 2020, Ebrahimi *et al*. 2020, 2021d, Dabbagh *et al*. 2020). Noted that CNTRC and its grading are considered a sufficient example for the numerical analysis of this work but it cannot capture agglomeration and waviness adverse effect. However, all previous studies neglected the effect of grading index and CNT orientation angle on the beam response and analysis results. Both are considered on the presented unified model on this paper as added value for its broad capabilities.

However, some previous studies tried to perform generalization or unification of beams FE modeling such as (Lees and Thomas 1982, Nabi and Ganesan 1994, Li 2008), the perspective of each differs from one proposed in this research. For example, Lees and Thomas (1982) tried to present a new formulation with huge variable numbers in a hierarchical structure to obtain different required accuracy. They also consider that all other FE models existed were just exceptional cases from their unified element. This study considered isotropic beams only without further consideration for another material type. Nabi and Ganesan (1994) studied FE modeling generalization from the loading point of view, especially for composite beams. They considered bi-axial bending and torsion, which required 16 degrees of freedom per element to achieve. Li (2008) introduced a unified FE approach to treat FGM beams as well as layered beams and compared between them. Different governing theories were used in the literature, starting from classical to reach refined high order beam theories. Also, various degrees of freedom and element formulations were considered in many types of research. This study chose a simple Timoshenko beam element with two nodes and 6 degrees of freedom to achieve the required accuracy and generalization without any complications in derivations and mathematical representations.

This research aims to unify the FE modeling of isotropic, orthotropic, FGM, nanocomposite and FG nanocomposite beams. That is why a simple 1-D Timoshenko beam element is chosen. The shape function is the vital formula representing the interpolation of the field variables and overall model accuracy and efficiency. Therefore, the presented model shape function is not conventional, where it depends on both beam geometry and material properties to cover all chosen material aspects. The FE formulations for beam modeling are investigated based on TBT. Research starts with mathematical formulations and element explanation. The detailed derivation is performed to obtaining the unified shape function and the difference between traditional and presented ones. The methodology for obtaining stiffness, mass and corresponding equations of motion are mentioned. Model general aspects are also explained, such as convergence, shape function, unique characteristics and free-off shear locking. Both static and free vibration responses are studied and compared with previously published. Numerical analysis is performed for different beams made of all introduced materials. Results show broad capabilities and acceptable accuracy for the presented model. The proposed approach relaxes the FEM constraints on the structural material modeling and enhanced analysis ability to keep up with the fast material development on structural engineering.

2. Beam definition & theoretical background

The following section illustrates the proposed beam's geometric characteristics and the construction of the presented element. Together with these, the underlying theory and governing equations for the derivation are also stated.

The Beam origin of the coordinates located at mid-points of length, width and thickness (L, b and h respectively) and the selected element contain two-node each has three degrees of freedom u_i, w_i, ϕ_i based on (Chakraborty *et al*. 2003). The simple form of rule-of-mixture Eq. (1) is used to obtain composite properties from its constituent materials of fibers and polymer-matrix as (Gibson 2016).

$$\begin{aligned} &E_1^c = V_f E_1^f + V_m E^m, \qquad \frac{1}{E_2^c} = \frac{V_f}{E_2^f} + \frac{V_m}{E^m} \\ &\frac{1}{G_{12}^c} = \frac{V_f}{G_{12}^f} + \frac{V_m}{G^m}, \qquad \upsilon_{12}^c = V_f \upsilon_{12}^f + V_m \upsilon^m \\ &\upsilon_{21}^c = \frac{\upsilon_{12}^c}{E_1^c} E_2^c, \qquad \rho^c = V_f \rho^f + V_m \rho^m \\ &V_m = 1 - V_f \end{aligned} \tag{1}$$

V_f and V_m are the fiber and matrix volume fractions. E_1^f, E_2^f, G_{12}^f, *and* υ_{12}^f are fiber modulus of elasticity in 1,2 direction, shear modulus in 12 plane and Poisson's ratio in 12 plane, respectively. Also, the same parameters for matrix have superscript$m$and composite with c sign.

FGM grading concept follows the power law governing theory (El-Ashmawy *et al*. 2016). Eq. (2) and Fig. 1 illustrates the power-law function and effect of power-law index n on the properties change along the thickness direction.

$$P(z) = (P_t - P_b)\left(\frac{z}{h} + \frac{1}{2}\right)^n + P_b \quad \left(-\frac{h}{2} \le z \le \frac{h}{2}\right) \tag{2}$$

Wherein gradient index n is the parameter defined the shape and the slope of changed material properties through the thickness. Note that P_t *and* P_b are the beam's properties in the top-most and bottom-most layer.

The extended rule of mixture (Shen 2009) is used to calculate CNTRC properties. Properties and parameters of CNT and matrix are noted by CNT and m as Eq. (3).

$$E_{11} = \eta_1 V_{CNT} E_{11}^{CNT} + V_m E^m, \qquad \frac{\eta_2}{E_{22}} = \frac{V_{CNT}}{E_{22}^{CNT}} + \frac{V_m}{E^m} \tag{3}$$

$$\frac{\eta_3}{G_{12}} = \frac{V_{CNT}}{G_{12}^{CNT}} + \frac{V_m}{G^m}, \qquad \upsilon_{12} = V_{CNT}\upsilon_{12}^{CNT} + V_m\upsilon^m$$
$$\upsilon_{21} = \frac{\upsilon_{12}}{E_{11}}E_{22}, \qquad \rho = V_{CNT}\rho^{CNT} + V_m\rho^m$$
$$V_m = 1 - V_{CNT}$$

The efficiency parameters η_1, η_2, and η_3 for CNT/ matrix combination are studied by comparing the elastic properties results of molecular dynamic simulations with the calculated by extended rule of mixture for specific CNT total volume fraction V_{tcnt}. Selected values of V_{tcnt} as described in (Han and Elliott 2007, Ansari *et al.* 2014) and corresponding efficiency parameters are tabulated in Table 1.

Graphene Nanoplatelet-Reinforced Composite (GPLRC) modulus of elasticity is assumed as homogeneous isotropic material and estimated using the Halpin-Tsai micro-mechanics model as Eq. (4). Where η_L, η_T are reduction parameters, ζ_L, ζ_T are geometric factors, a_{GPL}, b_{GPL}, and t_{GPL} are the length, width and thickness for GPLs, respectively. Other properties such as Poisson's ration and density are calculated as the conventional rule of mixture stated in Eq. (3).

$$E = \frac{3}{8}\frac{1+\zeta_L\eta_L V_{GPL}}{1-\eta_L V_{GPL}}E^m + \frac{5}{8}\frac{1+\zeta_T\eta_T V_{GPL}}{1-\eta_T V_{GPL}}E^m$$
$$Where,$$
$$\eta_L = \frac{(E^{GPL}/E^m)-1}{(E^{GPL}/E^m)+\zeta_L}, \qquad \eta_T = \frac{(E^{GPL}/E^m)-1}{(E^{GPL}/E^m)+\zeta_T} \tag{4}$$
$$\zeta_L = 2(a_{GPL}/t_{GPL}), \qquad \zeta_T = 2(b_{GPL}/t_{GPL})$$

For FG-CNTRC and FG-GPLRC adapted power-law is used as Eq. (5). V_{tcnt} and V_{tgpl} are the total volume fractions of CNT and GPL. As an example, CNT volume fraction V_{CNT} changing with $n$is showed in Fig. 2.

$$V_{CNT}(z) = (n+1)\left(\frac{1}{2}-\frac{z}{\hbar}\right)^n V_{tcnt} \quad \left(-\frac{\hbar}{2} \le z \le \frac{\hbar}{2}\right)$$
$$V_{GPL}(z) = (n+1)\left(\frac{1}{2}-\frac{z}{\hbar}\right)^n V_{tgpl} \quad \left(-\frac{\hbar}{2} \le z \le \frac{\hbar}{2}\right) \tag{5}$$

3. The constituent material modeling & governing equations

Starting from displacement-field based on TBT, governing differential equations are derived. The process arranges as the strain-displacement field, stress-strain relationship, virtual energies formulations, then applying Hamilton's principle to find governing differential equations. The plan-stress approximations are assumed. Also, Y-direction is estimated to be stress-free. Moreover, zero external work is considered in energy formulations.

3.1 The constituent material modeling

Based on TBT, axial displacement $u(x,z)$ and transverse $w(x,z)$are expressed in Eq. (6).

$$u(x,z) = u_0(x) - z\phi(x), \qquad w(x,z) = w_0(x) \tag{6}$$

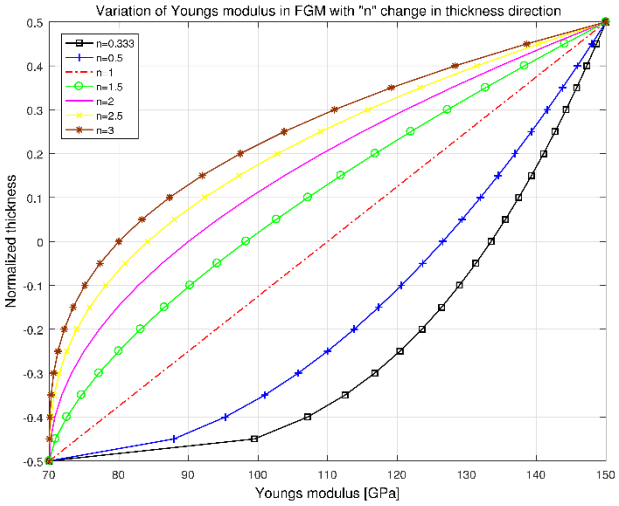

Fig. 1 Properties variation of FGM in thickness direction using power-law

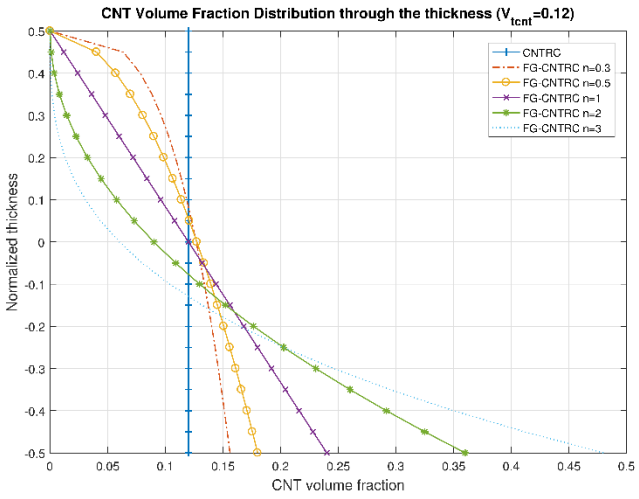

Fig. 2 V_{CNT} distributions through the normalized thickness according to power-law for CNTRC and FG-CNTRC

Table 1 V_{tcnt} selected values and corresponding efficiency parameters

V_{tcnt}	η_1	η_2	η_3
0.12	0.137	1.022	0.715
0.17	0.142	1.626	1.138
0.28	0.141	1.585	1.109

u_0 and w_0 are initial mid-plane axial and transverse displacement. ϕ is slope or rotation displacement.

For strain-displacement field, the extensional strain along x-direction ε_{xx} and in-plane shear strain γ_{xz} are derived in Eq. (7), then putted in matrix form in Eq. (8). ε_{xx}^0, γ_{xz}^0, and k_{xx}^0 are the reference extensional strain, shear strain and curvature, respectively.

$$\varepsilon_{xx} = \frac{\partial u_0}{\partial x} - z\frac{\partial \phi}{\partial x} = \varepsilon_{xx}^0 - zk_{xx}^0 \tag{7}$$

$$\gamma_{xz} = -\phi + \frac{\partial w_0}{\partial x} = \gamma_{xz}^0$$

$$\begin{Bmatrix}\varepsilon_{xx}\\ \gamma_{xz}\end{Bmatrix} = \begin{Bmatrix}\varepsilon_{xx}^0\\ \gamma_{xz}^0\end{Bmatrix} + z\begin{Bmatrix}k_{xx}^0\\ 0\end{Bmatrix} \tag{8}$$

Stress-strain relationship is found using Hook's law in general form Reddy (2003) as Eq. (9), where $i,j = 1{:}\,6$and $k,l = 1{:}\,3$.

$$\sigma_{ij} = C_{ijkl}\varepsilon_{kl} \tag{9}$$

Transverse directional stress component σ33 is removed by applying plan-stress assumptions Reddy (2003) and eliminating the corresponding strain ε_{33}. Eq. (10) represents the reduced form of Eq. (9). Q_{ij} is the stiffness components.

$$\begin{Bmatrix}\sigma_{11}\\ \sigma_{22}\\ \sigma_{23}\\ \sigma_{13}\\ \sigma_{12}\end{Bmatrix} = \begin{bmatrix}Q_{11} & Q_{12} & 0 & 0 & 0\\ Q_{21} & Q_{22} & 0 & 0 & 0\\ 0 & 0 & Q_{44} & 0 & 0\\ 0 & 0 & 0 & Q_{55} & 0\\ 0 & 0 & 0 & 0 & Q_{66}\end{bmatrix}\begin{Bmatrix}\varepsilon_{11}\\ \varepsilon_{22}\\ \varepsilon_{23}\\ \varepsilon_{13}\\ \varepsilon_{12}\end{Bmatrix} \tag{10}$$

Stiffness components depend on engineering parameters for each material as a separate case.

• For isotropic materials and GPLRC:

$$\begin{aligned} &Q_{11} = Q_{22} = \frac{E}{1-\upsilon^2}, \qquad Q_{12} = \frac{\upsilon E}{1-\upsilon^2}\\ &Q_{44} = Q_{55} = Q_{66} = G \end{aligned} \tag{11}$$

• For orthotropic (layered-fiber composite) materials: (knotation for layer number)

$$\begin{aligned} &Q_{11}^k = \frac{E_1^k}{1-\upsilon_{12}^k\upsilon_{21}^k}, \qquad Q_{22}^k = \frac{E_2^k}{1-\upsilon_{12}^k\upsilon_{21}^k}\\ &Q_{12}^k = \frac{\upsilon_{12}^k E_2^k}{1-\upsilon_{12}^k\upsilon_{21}^k}, \qquad Q_{44}^k = Q_{23}^k\\ &Q_{55}^k = G_{13}^k, \qquad Q_{66}^k = G_{12}^k \end{aligned} \tag{12}$$

• For FGM and FG-GPLRC: (material properties are function in z-direction)

$$\begin{aligned} &Q_{11} = Q_{22} = \frac{E(z)}{1-\upsilon^2(z)}, \qquad Q_{12} = \frac{\upsilon(z)E(z)}{1-\upsilon^2(z)}\\ &Q_{44} = Q_{55} = Q_{66} = G(z) \end{aligned} \tag{13}$$

• For CNTRC: (as one layer)

$$\begin{aligned} &Q_{11} = \frac{E_1}{1-\upsilon_{12}\upsilon_{21}}, \qquad Q_{22} = \frac{E_2}{1-\upsilon_{12}\upsilon_{21}}\\ &Q_{12} = \frac{\upsilon_{12}E_2}{1-\upsilon_{12}\upsilon_{21}}, \qquad Q_{44} = G_{23}\\ &Q_{55} = G_{13}, \qquad Q_{66} = G_{12} \end{aligned} \tag{14}$$

• For FG-CNTRC:

$$\begin{aligned} &Q_{11} = \frac{E_1(z)}{1-\upsilon_{12}(z)\upsilon_{21}(z)}, \qquad Q_{22} = \frac{E_2(z)}{1-\upsilon_{12}(z)\upsilon_{21}(z)}\\ &Q_{12} = \frac{\upsilon_{12}(z)E_2(z)}{1-\upsilon_{12}(z)\upsilon_{21}(z)}, \qquad Q_{44} = G_{23}(z)\\ &Q_{55} = G_{13}(z), \qquad Q_{66} = G_{12}(z) \end{aligned} \tag{15}$$

Transformation form principal axes 1, 2 and 6 into geometrical axes x, y and z is performed to compensate orientations if exists. Eq. (10) transforms to Eq. (16) and $\overline{Q}_{ij}$ is the transformed stiffness component.

$$\begin{Bmatrix}\sigma_{xx}\\ \sigma_{yy}\\ \sigma_{yz}\\ \sigma_{xz}\\ \sigma_{xy}\end{Bmatrix} = \begin{bmatrix}\overline{Q}_{11} & \overline{Q}_{12} & 0 & 0 & \overline{Q}_{16}\\ \overline{Q}_{12} & \overline{Q}_{22} & 0 & 0 & \overline{Q}_{26}\\ 0 & 0 & \overline{Q}_{44} & \overline{Q}_{45} & 0\\ 0 & 0 & \overline{Q}_{45} & \overline{Q}_{55} & 0\\ \overline{Q}_{16} & \overline{Q}_{26} & 0 & 0 & \overline{Q}_{66}\end{bmatrix}\begin{Bmatrix}\varepsilon_{xx}\\ \varepsilon_{yy}\\ \gamma_{yz}\\ \gamma_{xz}\\ \gamma_{xy}\end{Bmatrix} \tag{16}$$

Y-direction is stress-free. By put its corresponding normal and shear strain values equal to zeros, a reduced form is found as Eq. (17).

$$\begin{Bmatrix}\sigma_{xx}\\ \sigma_{xz}\end{Bmatrix} = \begin{bmatrix}\tilde{Q}_{11} & 0\\ 0 & k_s\tilde{Q}_{55}\end{bmatrix}\begin{Bmatrix}\varepsilon_{xx}\\ \gamma_{xz}\end{Bmatrix} \tag{17}$$

k_s is the shear correction factor and $\tilde{Q}_{ij}$ is the reduced transformed stiffness components and can be calculated for each material as follows.

For isotropic and GPLRC materials:

$$\tilde{Q}_{11} = E, \qquad and\ \tilde{Q}_{55} = G$$

For layered-fiber composite and CNTRC:

$$\tilde{Q}_{11} = \overline{Q}_{11} - \frac{\overline{Q}_{12}^2}{\overline{Q}_{22}}, \qquad and\ \tilde{Q}_{55} = \overline{Q}_{55}$$

For FGM and FG-GPLRC:

$$\tilde{Q}_{11} = E(z), \qquad and\ \tilde{Q}_{55} = G(z)$$

For FG-CNTRC:

$$\tilde{Q}_{11} = \overline{Q}_{11}(z) - \frac{\overline{Q}_{12}^2(z)}{\overline{Q}_{22}(z)}, \qquad and\ \tilde{Q}_{55} = \overline{Q}_{55}(z)$$

3.2 Governing equations

The kinetic T and strain Uenergies (Khdeir and Reddy 1997) of the beam structure are given by Eqs. (18) and (19).

$$T = \frac{1}{2}\int_V \rho[\dot{u}^2 + \dot{w}^2]\,dV \tag{18}$$

$$U = \frac{1}{2}\int_V (\sigma_{xx}\varepsilon_{xx} + \sigma_{xz}\gamma_{xz})\,dV \tag{19}$$

Virtual strain energy is expressed by inserting Eq. (7) into Eq. (19) and introducing integrated stiffness coefficients as (Chakraborty *et al*. 2003, El-Ashmawy *et al*. 2016) as Eq. (20).

$$\begin{aligned} &[A_{11} \quad B_{11} \quad D_{11}] = \int_A \tilde{Q}_{11}[1 \quad z \quad z^2]dA\\ &[A_{55}] = \int_A k_s\tilde{Q}_{55}\,dA \end{aligned} \tag{20}$$

The final form of the virtual strain energy δU is stated in Eq. (21).

$$\delta U = \frac{1}{2}\int_0^L \begin{bmatrix} \left(A_{11}\frac{\partial^2 u_0}{\partial x^2} - B_{11}\frac{\partial^2\phi}{\partial x^2}\right)\delta u_0\\ -\left(B_{11}\frac{\partial^2 u_0}{\partial x^2} - D_{11}\frac{\partial^2\phi}{\partial x^2} - A_{55}\phi + A_{55}\frac{\partial w_0}{\partial x}\right)\delta\phi\\ +\left(-A_{55}\frac{\partial\phi}{\partial x} + A_{55}\frac{\partial^2 w_0}{\partial x^2}\right)\delta w_0 \end{bmatrix} dx \tag{21}$$

Also, integrated mass coefficients I_0, I_1, and I_2 as

(Chakraborty *et al*. 2003, El-Ashmawy *et al*. 2016) are showed in Eq. (22).

$$[I_0 \quad I_1 \quad I_2] = \int_A \rho\,[1 \quad z \quad z^2]dA \tag{22}$$

Substituting Eq. (6) after differentiation with respect to time into Eq. (18) and utilizing Eq. (22), the final form of virtual kinetic energy δT is obtained as Eq. (23).

$$\delta T = \frac{1}{2}\int_0^L \left[\left(I_0\ddot{u}_0 - I_1\ddot{\phi}\right)\delta u_0 + \left(I_2\ddot{\phi} - I_1\ddot{u}_0\right)\delta\phi + (I_0\ddot{w}_0)\delta w_0\right]dx \tag{23}$$

Hamilton's principle is considered a dynamic version of the principle of virtual displacements. The governing differential Eqs. of the Timoshenko beam are derived using Hamilton's principal Eq. (24).

$$0 = \int_0^T (\delta U + \delta W - \delta T)\,dt \tag{24}$$

δW is the virtual work done by the applied forces. Zero external work should be assumed to drive the Eqs of motion $\delta W = 0$. Differential Eq.s of motion are derived in terms of three-degrees of freedom $u_0,\ w_0,\ and\ \phi$ as Eq. (25), respectively.

$$\begin{aligned} I_0\ddot{u}_0 - I_1\ddot{\phi} - A_{11}\frac{\partial^2 u_0}{\partial x^2} + B_{11}\frac{\partial^2\phi}{\partial x^2} &= 0 \\ I_0\ddot{w}_0 + A_{55}\frac{\partial\phi}{\partial x} - A_{55}\frac{\partial^2 w_0}{\partial x^2} &= 0 \\ I_2\ddot{\phi} - I_1\ddot{u}_0 + B_{11}\frac{\partial^2 u_0}{\partial x^2} - D_{11}\frac{\partial^2\phi}{\partial x^2} - A_{55}\phi + A_{55}\frac{\partial w_0}{\partial x} &= 0 \end{aligned} \tag{25}$$

4. A material-dependent shape function & FE formulations

4.1 A material-dependent shape function

The ordinary static part of Eq. (25) are solved. The exact solution is found in Eq. (26). c_i is polynomial constant.

$$\begin{aligned} u_0 &= c_1 + c_2x + c_3x^2 \\ w_0 &= c_4 + c_5x + c_6x^2 + c_7x^3 \\ \phi &= c_8 + c_9x + c_{10}x^2 \end{aligned} \tag{26}$$

As Eq. (26), the order of w_0 interpolation is one order higher than the slope ϕ. This condition is one of the elements' requirements to be free of shear-locking. It increases the element ability to accurately model the curvature present in the actual material under bending and shear stress. The exact solution for the displacement has ten constants and only six boundary conditions, three degrees of freedom at each node of the element, are available. Hence, there are only six independent constants. The additional four dependents are expressed in terms of six other independent constants by substituting Eqs. (26) into (25) and solving the following relations, Eqs. (27) is found.

$$c_3 = \frac{\alpha(c_8 - c_5)}{2}, \qquad c_6 = \frac{c_9}{2} \tag{27}$$

$$c_7 = \frac{\beta(c_8 - c_5)}{6}, \qquad c_{10} = 3c_7$$

α and β are related to the coupling among stiffness coefficients and equal to Eq. (28).

$$\alpha = \frac{B_{11}A_{55}}{(A_{11}D_{11} - B_{11}^2)}, \qquad \beta = \frac{A_{11}A_{55}}{(A_{11}D_{11} - B_{11}^2)} \tag{28}$$

The reduction in displacement reaches only six constants as Eq. (29). It is written in matrix form as Eq. (30).

$$\begin{aligned} u_0 &= c_1 + c_2x + \frac{1}{2}\alpha(c_8 - c_5)x^2 \\ w_0 &= c_4 + c_5x + \frac{1}{2}c_9x^2 + \frac{1}{6}\beta(c_8 - c_5)x^3 \\ \phi &= c_8 + c_9x + \frac{1}{2}\beta(c_8 - c_5)x^2 \end{aligned} \tag{29}$$

$$\begin{Bmatrix} u_0 \\ w_0 \\ \phi \end{Bmatrix} = \begin{bmatrix} 1 & x & 0 & -\frac{1}{2}\alpha x^2 & \frac{1}{2}\alpha x^2 & 0 \\ 0 & 0 & 1 & x - \frac{1}{6}\beta x^3 & \frac{1}{6}\beta x^3 & \frac{1}{2}x^2 \\ 0 & 0 & 0 & -\frac{1}{2}\beta x^2 & 1 + \frac{1}{6}\beta x^2 & x \end{bmatrix} \begin{Bmatrix} c_1 \\ c_2 \\ c_4 \\ c_5 \\ c_8 \\ c_9 \end{Bmatrix} = [N(x)]\{a\} \tag{30}$$

$[N(x)]$ is the matrix containing functions of x and $\{a\}$is the column vector of independent constants. Applying the element boundary condition at node 1 $(x = 0)$ and node 2 $(x = L)$, Eq. (31) is defined nodal displacement vector for the element $\{\hat{u}\}$.

$$\{\hat{u}\} = \begin{Bmatrix} u_1 \\ w_1 \\ \phi_1 \\ u_2 \\ w_2 \\ \phi_2 \end{Bmatrix} = \begin{bmatrix} N(0) \\ N(L) \end{bmatrix}\{a\} = [g]^{-1}\{a\}, then \tag{31}$$
$$\{a\} = [g]\{\hat{u}\}$$

Then, the displacement at any point Eq. (32) is expressed in terms of nodal displacement by substituting Eq. (31) into (30).

$$\begin{Bmatrix} u_0 \\ w_0 \\ \phi \end{Bmatrix} = [N(x)]\{a\} = [N(x)][g]\{\hat{u}\} = [X(x)]\{\hat{u}\} \tag{32}$$

$[X(x)] = [X^u(x) \quad X^w(x) \quad X^\phi(x)]^T$ are the exact shape functions for axial, transverse and rotational degrees of freedom, respectively. Detailed shape functions are listed in Eq. (34). A simplification parameter, ψ is defined in Eq. (33)

$$\psi = \frac{1}{12 + \beta L^2} \tag{33}$$

$$\begin{aligned} X_{11}^u &= (1 - x/L), \qquad X_{12}^u = -X_{15}^u = \frac{6\psi\alpha x(x - L)}{L} \\ X_{13}^u &= -X_{16}^u = 3\psi\alpha x(x - L), \qquad X_{14}^u = (x/L) \\ X_{11}^w &= X_{14}^w = 0 \\ X_{12}^w &= \frac{\psi(\beta L^3 - 3\beta L x^2 + 12L + 2\beta x^3 - 12x)}{L} \end{aligned} \tag{34}$$

$$X_{13}^{w}=\frac{\psi x(\beta L^3-2\beta L^2x+\beta Lx^2+6L-6x)}{L}$$
$$X_{15}^{w}=\frac{\psi x(-2\beta x^2+3L\beta x+12)}{L}$$
$$X_{16}^{w}=\frac{-\psi x(\beta L^2x-\beta Lx^2+6L-6x)}{L}$$
$$X_{11}^{\phi}=X_{14}^{\phi}=0,\qquad X_{12}^{\phi}=-X_{15}^{\phi}=\frac{-6\psi\beta x(L-x)}{L}$$
$$X_{13}^{\phi}=\frac{\psi(\beta L^3-4\beta L^2x+3\beta Lx^2+12L-12x)}{L}$$
$$X_{16}^{\phi}=\frac{\psi x(-2\beta L^2+3\beta xL+12)}{L}$$

4.2 FE formulations

From strain-displacement relationship illustrated in section 3.1, strain is derived as Eq. (35).

$$\{\varepsilon\}=\begin{bmatrix}\frac{\partial}{\partial x} & 0 & -z\frac{\partial}{\partial x}\\ 0 & \frac{\partial}{\partial x} & -1\end{bmatrix}\{u\}=[d][X]\{\hat{u}\}=[B]\{\hat{u}\} \tag{35}$$

$[d]$ is a differential operator matrix and $[B]=[d][X]$ is a parameter used to deduce elementary stiffness matrix $[K]_e$ as Eq. (36) (Caraballo 2011).

$$[K]_e=\int_V [B]^T[\tilde{Q}][B]dV \tag{36}$$

After matrices multiplying, integration and using the definitions in Eq. (20), element stiffness matrix is found in closed form. The consistent elements of the mass matrix are computed as a sum of four sub-matrices deduced from the dynamic part of motion Eq. (25), $[M]=[M_u]+[M_w]+[M_\phi]+[M_{u\phi}]$ where they represent $u, w, \phi,\ and\ u\&\phi$ coupling contributions in mass matrix. They are summarized in Eq. (37).

$$[M_u]=\int_0^L I_0[X_u]^T[X_u]dx,\qquad [M_w]=\int_0^L I_0[X_w]^T[X_w]dx$$
$$[M_\phi]=\int_0^L I_2[X_\phi]^T[X_\phi]dx \tag{37}$$
$$[M_{u\phi}]=-\int_0^L I_1\left([X_u]^T[X_\phi]+[X_\phi]^T[X_u]\right)dx$$

Performing the matrix multiplying, integration and using the definitions in shape function Eq. (34) element mass matrix is derived. Distributed load as a force element is expressed as Eq. (38). $\{P_{b_t}\}_e$ is the element distributed load vector and f_t is the transverse distributed load function along the length.

$$\{P_{b_t}\}_e=\int_0^L f_t[X_w]^Tdx=\left\{0\quad \frac{f_tL}{2}\quad \frac{f_tL^2}{12}\quad 0\quad \frac{f_tL}{2}\quad \frac{-f_tL^2}{12}\right\}^T \tag{38}$$

Finally, obtained matrices are inserted in the governing Eq. of motion as Eq. (39).

$$[M]\{\ddot{\hat{u}}\}+[K]\{\hat{u}\}=\{F\} \tag{39}$$

4.3 Model features

Previously, shape functions contain only element length L as a variable parameter. Nowadays, it represents a challenge in modeling advanced material such as FGM. The presented unified shape function depends on $\alpha and \beta$ in addition to L. Mentioned parameters are function of material and geometry as stated in Eqs. (28), (20) and (17). This factor increases the ability of shape function to present various advanced materials behavior, even continuously-changed properties like FGM.

Moreover, lateral deflection interpolation is assumed to be cubic polynomial on the displacement function and higher-order than axial and rotational displacement as Eq. (26). As well, many length-to-thickness ratios L/h are checked to ensure that the model avoided a significant increase in beam stiffness with a larger L/h. Both cubic interpolation and the ability of long beams analysis secure the model from shear locking or bending errors. Moreover, the used Hermite interpolation provides inter-element continuity of the displacement field and its first derivatives at nodes. Therefore, the introduced element achieves C^1 high-precious degree of continuity.

Model convergence is investigated for each material case, as follows later in results & analysis in section 5. It is concluded that one element is sufficient to converge static analysis results or super convergence. This feature is existed because the displacement field is accurately derived from the governing Eqs.' static part and the sequence stiffness matrix. It is precisely for the loading point and behaved like the direct stiffness method. This property also reduces calculations time, which in turn minimizes the computational cost. Nevertheless, the mass matrix had approximations, as it is approximately deduced from the dynamic part and did not represent the exact solution. That is the reason for the slower convergence in the dynamic analysis case.

5. Results & analysis

The following sections investigates convergence, static and dynamic response to the selected types of materials. Isotropic beams are represented by Aluminum, orthotropic by fiber composites and FG beams by Aluminum/Zirconia. Nanocomposite example is chosen to be CNTRC and FG-CNTRC. The boundary conditions are considered as following, Fixed-Fixed (F-F) $u(0)=u(L)=w(0)=w(L)=\phi(0)=\phi(L)=0$, for Fixed-Simply Supported (F-SS) $u(0)=w(0)=w(L)=\phi(0)=0$, then SS-SS$u(0)=w(0)=w(L)=0$, F-Free $u(0)=w(0)=\phi(0)=0$. The shear correction factor is chosen equals to $k_s=5/6$. Different length-to-thickness ratios L/h is chosen to check analysis results and model accuracy for short and long beams.

5.1 Isotropic beam

5.1.1 Static deflection

The presented model static-convergence is checked for the aluminum beam having geometric and material properties listed in Table 2, subjected to constant distributed-load equals 1 N/m and $L/h=10$. Normalization is conducted according to $\bar{w}=\left(w10^2/EI_{yy}L^4\right)$. The normalized tip

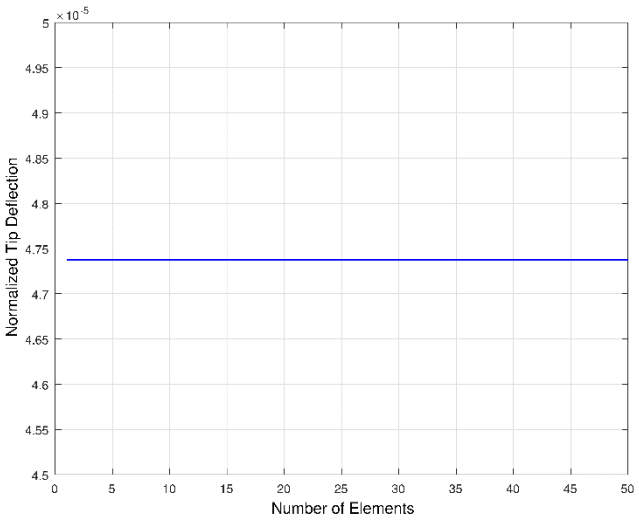

Fig. 3 Normalized tip deflection convergence of F-Free aluminum beam

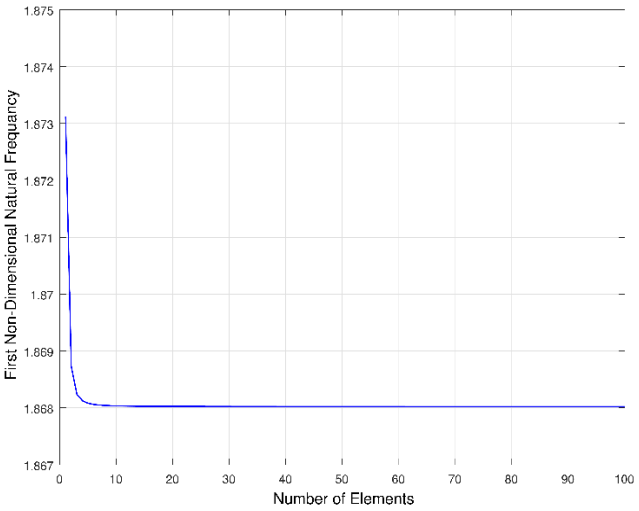

Fig. 4 First dimensionless natural frequency versus NE of cantilever aluminum beam

Table 2 Aluminum beam geometric and material characteristics

Property	Aluminum	Unit
E	68.9	GPa
υ	0.25	-
G	27.6	GPa
ρ	2769	kg/m^3
L	0.1524	m
b	0.0254	m
h	0.01524	m

Table 3 Transverse tip displacement of isotropic F-Free beam subjected to various distributed load values

f_t [N/m]	Unified Model	FE (Elshafei 2013)	Exact TBT (Friedman and Kosmatka 1993)
1	240,240	240,550	240,612
2	480,480	481,100	481,224
3	720,720	721,650	721,836
4	960,960	962,200	692,448
5	1,201,200	1,202,800	1,203,060
6	1,441,400	1,443,300	1,443,672
7	1,681,700	1,683,900	1,684,284
8	1,921,900	1,924,400	1,924,896
9	2,162,200	2,165,000	2,165,508
10	2,402,400	2,405,500	2,406,120

deflection convergence for cantilever beam is studied in Fig. 3. The super-convergence property is clearly seen for the static analysis prediction of the proposed model.

The same beam but with standard geometric and material properties as (Friedman and Kosmatka 1993, Elshafei 2013) is chosen to ensure model ability of accurately analyze isotropic beam element. Typical beam properties are $L/h = 20,\ h = b = 1,\ E = 1,\ \upsilon = 1$ and $f_t = 1{:}\,10$N/m. Table 3 lists the obtained results comparison

Table 4 Non-dimensional frequencies $\bar{\omega}$ of F-F aluminum beam

Theory	L/h	$\bar{\omega}_1$	$\bar{\omega}_2$	$\bar{\omega}_3$	$\bar{\omega}_4$	$\bar{\omega}_5$
Unified Model	20	4.6920	7.7109	10.6573	13.4940	14.7556
FE (Elshafei 2013)		4.6937	7.7169	10.6705	13.5167	14.7532
FOSDT (Kocatürk and Şimşek 2005)		4.6898	7.7035	10.6399	13.4611	16.1586
TOSDT (Şimşek and Kocatürk 2007)		4.6902	7.7052	10.6447	13.4703	16.1754
CBT (Lee and Schultz 2004)		4.6899	7.7035	10.6401	13.4611	16.1590
Unified Model	100	4.7285	7.8472	10.9809	14.1080	17.2280
FE (Elshafei 2013)		4.7324	7.8615	11.0150	14.1745	17.3424
FOSDT (Kocatürk and Şimşek 2005)		4.7283	7.8468	10.9799	14.1061	17.2244
TOSDT (Şimşek and Kocatürk 2007)		4.7284	7.8569	10.9801	14.1064	17.2249
CBT (Lee and Schultz 2004)		4.7284	7.8469	10.9800	14.1062	17.2246

with previously published. A good agreement is noticed, an error percentage with exact solution Friedman and Kosmatka (1993) did not exceed 0.16%.

5.1.2 Natural frequencies

The first natural frequency convergence is tested for a F-Free aluminum beam with properties given as Table 2. The non-dimensional natural frequencies is defined as $\bar{\omega}_i = \omega_i L^2 \sqrt{\frac{\rho A}{EI}}$. Fig. 4 shows that the first dimensionless natural frequency started to converge at a suitable Number of Elements (NE). The dynamic behavior differs from the static one where the prediction delayed in convergence because of the mass matrix approximations effect.

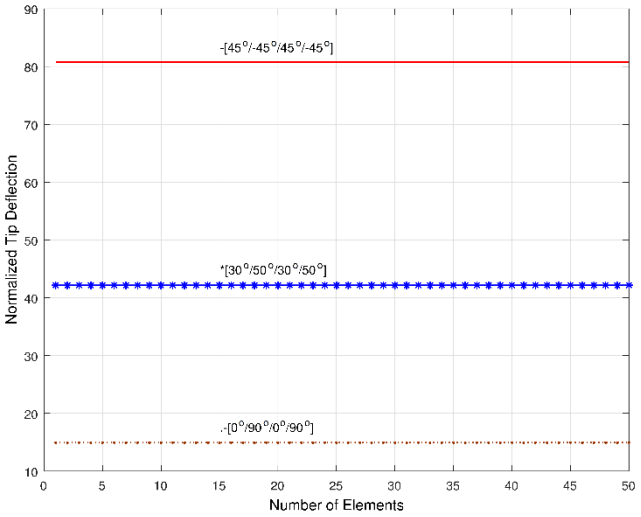

Fig. 5 Convergence of normalized transverse tip deflection of multi-oriented cantilever orthotropic beam

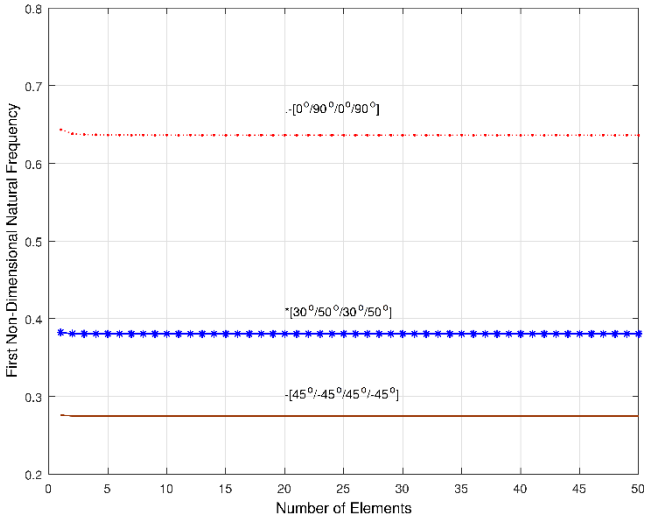

Fig. 6 First non-dimensional natural frequency vs. NE for cantilever composite beams

Table 5 Normalized mid-span deflection of symmetric composite beams with various boundary conditions

Theory	L/h	SS-SS	F-SS	F-F	F-Free
Unified Model	10	0.9480	0.6084	0.4296	3.1033
FE (Elshafei 2013)		1.1383	0.7825	0.5694	2.4221
HOSDT (Khdeir and Reddy 1997)		1.0960	0.7400	0.5320	3.4550
SOSDT (Khdeir and Reddy 1997)		0.9590	0.6220	0.4420	3.1350
FOSDT (Khdeir and Reddy 1997)		1.0210	0.6930	0.5040	3.3230
RFOSDT (Chakraborty *et al*. 2002)		1.0200	0.6930	0.5040	3.3210
CBT (Khdeir and Reddy 1997)		0.6460	0.2590	0.1290	2.1980
Unified Model	50	0.6600	0.2735	0.1416	2.2393
FE (Elshafei 2013)		0.7268	0.3077	0.1584	1.1878
HOSDT (Khdeir and Reddy 1997)		0.6650	0.2800	0.1470	2.2510
SOSDT (Khdeir and Reddy 1997)		0.6590	0.2730	0.1420	2.2350
FOSDT (Khdeir and Reddy 1997)		0.6610	0.2760	0.1440	2.2430
RFOSDT (Chakraborty *et al*. 2002)		0.6600	0.2760	0.1440	2.2420
CBT (Khdeir and Reddy 1997)		0.6460	0.2590	0.1290	2.1980

The first five dimensionless-natural frequencies for F-F beam are compared to (Lee and Schultz 2004, Kocatürk and Şimşek 2005, Şimşek and Kocatürk 2007, Elshafei 2013) results in Table 4, where properties and geometry is the same $L/h = 20{,}100$ and $NE = 35$. The results assess the model analysis accuracy, as shown in Table 4, where FOSDT, SOSDT, TOSDT, HOSDT, RFOSDT and CBT are First, Second, Third, High, Refined First Order Shear Deformation and Classical Beam Theories. The obtained error margin between presented unified model and TOSDT Şimşek and Kocatürk (2007) is 0.04 : 8.78% for $L/h = 20$ and 0.002 : 0.02% for $L/h = 100$.

5.2 Orthotropic beam

5.2.1 Static deflection

A convergence test is performed for F-Free composite beam with normative material properties equal to $E_1^c/E_2^c = 25$, $G_{12}^c = 0.5E_2$, $\rho^c = 1$ and $v_{12}^c = 0.25$. The beam had different orientations with $L/h = 10$ and $f_t = 1\text{N/m}$. The tip deflection is normalized as shown in Fig. 5, according to $\bar{w} = \left(wAE^m h^2 10^2/f_t L^4\right)$.

A symmetric cross-ply$[0°/90°/0°]$ beam with the same mentioned material properties, different boundary conditions and $L/h = 10{,}50$, is compared with theories reported at (Khdeir and Reddy 1997, Chakraborty *et al*. 2002, Elshafei 2013) in Table 5. The mid-span deflection results vary among analysis theories and methods with acceptable margin. Wherein the obtained error margin between presented unified model and SOSDT Chakraborty *et al*. (2002) is 1 : 2.8% for $L/h = 10$ and 0.15 : 0.28% for $L/h = 50$.

5.2.2 Natural frequencies

The same beam with material properties and geometry as section 5.2.1 is chosen to check the convergence of dimensionless natural frequencies. Reasonable number of elements is required to converge, as illustrated in Fig. 6. Natural frequencies normalization is done according to $\bar{\omega}_i = \omega_i L^2 \sqrt{\frac{\rho^c}{E_1^c h^2}}$.

An AS/3501-6 graphite/epoxy is used to analyze free-vibration of composite beams. The following properties is calculated using Eq. (1), $E_1^c = 144.8\text{GPa}$, $E_2^c = 9.65\text{GPa}$, $G_{12}^c = 4.14\text{GPa}$, $v_{12}^c = 0.3$ and $\rho^c = 1389.23\text{Kg/m}^3$. Different orientations and boundary conditions are chosen with $L/h = 15$ and Laminates are assumed to be the same thickness and material. Table 6 represents the first non-dimensional natural frequency comparison with Ref. (Chandrashekhara *et al*. 1990, Chandrashekhara and Bangera 1992, Chakraborty *et al*. 2002, Elshafei 2013). Good agreement is concluded noted that in the second

Table 6 First dimensionless natural frequency of angle-ply and cross-ply composite beams with various boundary conditions

B.C	Unified Model	FE (Elshafei 2013)	Exact FOSDT (Chandrashekhara *et al*. 1990)	RFOSDT (Chakraborty *et al*. 2002)	HOSDT (Chandrashekhara and Bangera 1992)
θ			$[0°/90°/90°/0°]$		
SS-SS	2.4988	2.4864	2.4978	2.5070	2.5023
F-F	4.6603	4.5817	4.6602	4.6060	4.5940
F-SS	3.5486	3.5084	3.5446	3.5330	3.5254
F-Free	0.9220	0.9196	0.9231	0.9250	0.9241
θ			$[45°/-45°/-45°/45°]$		
SS-SS	0.9101	0.9033	1.5368	1.5260	0.8295
F-F	2.0525	1.9823	3.1843	3.1700	1.8472
F-SS	1.4179	1.3902	2.3032	2.2890	1.2855
F-Free	0.3256	0.3244	0.5551	0.5510	0.2965

Table 7 Mid-point dimensionless transverse deflection of FG beams with various power index, L/h=4 and16

Power Exponent	Theory	$\bar{w}$	
		$L/h = 4$	$L/h = 16$
$n = 0$ (Full Metal)	TBT (Simsek 2009)	1.13002	1.00812
	HOSDT (Simsek 2009)	1.15578	1.00975
	Unified Model	1.15600	1.00970
$n = 0.2$	TBT (Simsek 2009)	0.84906	0.75595
	HOSDT (Simsek 2009)	0.87145	0.75737
	Unified Model	0.86850	0.75680
$n = 0.5$	TBT (Simsek 2009)	0.71482	0.63953
	HOSDT (Simsek 2009)	0.73264	0.64065
	Unified Model	0.73080	0.64050
$n = 1$	TBT (Simsek 2009)	0.62936	0.56615
	HOSDT (Simsek 2009)	0.64271	0.56699
	Unified Model	0.64280	0.56700
$n = 2$	TBT (Simsek 2009)	0.56165	0.50718
	HOSDT (Simsek 2009)	0.57142	0.50780
	Unified Model	0.57330	0.50790

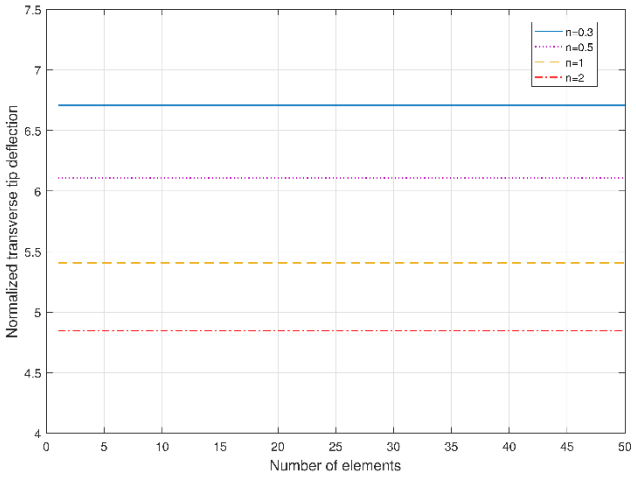

Fig. 7 Convergence of cantilever FG beam normalized tip deflection

orientation case there is high deviation in comparison with exact FOSDT and RFOSDT and equals or less than 11% for HOSDT due to cross-ply shear effect. Moreover, the obtained error margin between presented unified model and HOSDT (Chandrashekhara and Bangera 1992) is 0.14 : 1.4% for ply orientations $[0°/90°/90°/0°]$.

5.3 FG Beam

5.3.1 Static Deflection

A cantilever FG beam composed of Aluminum/ Zirconia is chosen for convergence and static deflection analysis. The top surface is aluminum with properties $E_{AL} = 70\text{GPa}$, $\upsilon_{AL} = 0.3$ and $G_{AL} = 27\text{GPa}$. Whereas, the bottom made of zirconia $E_{Zi} = 200\text{GPa}$, $\upsilon_{Zi} = 0.3$ and $G_{Zi} = 77\text{GPa}$. The material properties are changed along thickness according to power-law Eq. (2) subjected to $f_t = 1\text{N/m}$, $b = 0.1\text{m}$ and $L/h = 20$. The transverse deflection $\bar{w}$ is normalized by dividing into static displacement of fully aluminum beam as $w_{AL} = (5f_tL^4/384E_{AL}I)$. Fig. 7 shows convergence of tip normalized deflection with increasing NE for different power exponent n.

An SS-SS beam with the same properties and $L/h = 4, 16$ is used to compare maximum or mid-point dimension-

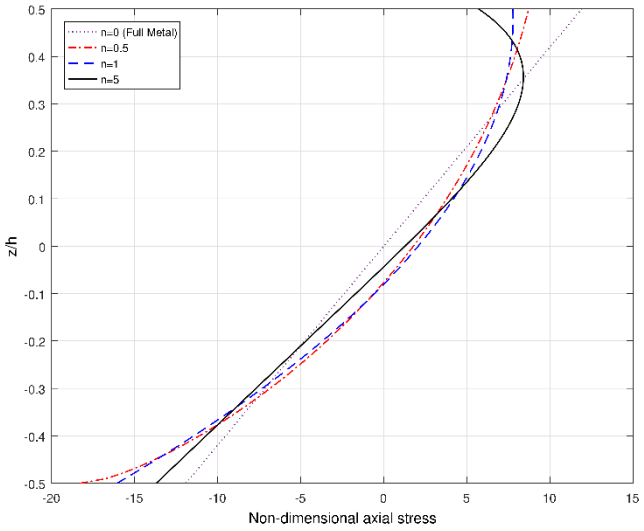

Fig. 8 Non-dimensional normal stress distributions for various n and $L/h = 16$

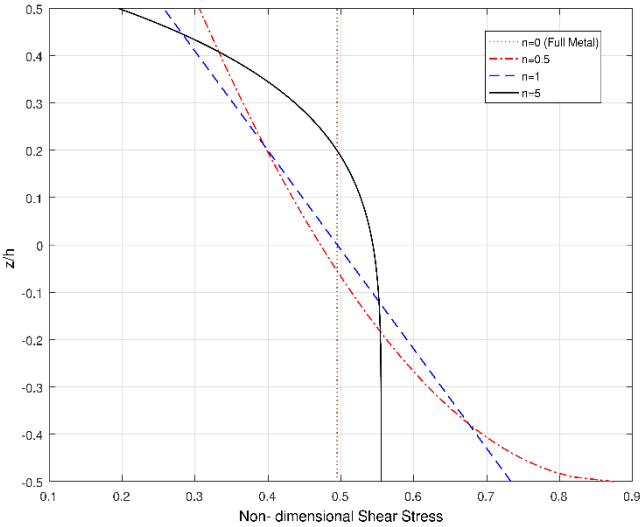

Fig. 9 Non-dimensional shear stress distributions for various n and $L/h = 16$

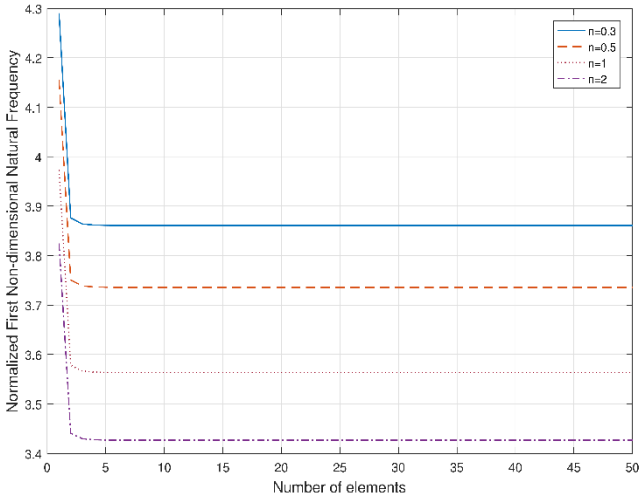

Fig. 10 Convergence of first non-dimensional natural frequency versus NE with various n and $L/h = 100$

Table 8 First non-dimensional natural frequencies for SS-SS beam with various L/h and n

L/h	Theory	$n=0$	$n=0.5$	$n=1$	$n=5$
5	Euler (Anandrao *et al*. 2012)	4.1845	3.7361	3.5639	3.2750
	TBT (Anandrao *et al*. 2012)	3.9338	3.5174	3.3509	3.0604
	Unified Model	3.9321	3.5164	3.3507	3.0599
10	Euler (Anandrao *et al*. 2012)	4.1845	3.7361	3.5639	3.2750
	TBT (Anandrao *et al*. 2012)	4.1178	3.6780	3.5072	3.2173
	Unified Model	4.1158	3.6764	3.5059	3.2160
20	Euler (Anandrao *et al*. 2012)	4.1846	3.7361	3.5639	3.2750
	TBT (Anandrao *et al*. 2012)	4.1690	3.7226	3.5507	3.2614
	Unified Model	4.1670	3.7208	3.5490	3.2599
50	Euler (Anandrao *et al*. 2012)	4.1846	3.7361	3.5639	3.2750
	TBT (Anandrao *et al*. 2012)	4.1838	3.7355	3.5632	3.2742
	Unified Model	4.1817	3.7336	3.5615	3.2726

less transverse deflection with (Simsek 2009) for different n, as shown in Table 7. The results clearly show that increasing n is accompanied by decreasing deflection with noticeable value. For all proposed n values and L/h, the error does not exceed 0.34% in comparison with HOSDT (Simsek 2009).

5.3.2 Stress analysis

Identical SS-SS FG beam to section 5.3.1 is proposed to study the stress distribution behavior of FGM. The normal stresses are calculated at $x = 0$ and normalized as $\bar{\sigma}_{xx} = \sigma_{xx}A/f_tL$. Whereas shear stress are obtained at $x = L/2$ and normalized as $\bar{\tau}_{xz} = \tau_{xz}A/f_tL$. The beam is subjected to distributed load $f_t = 1\text{N/m}$ and $L/h = 16$.

Figs. 8 and 9 show the dimensionless stress distributions against various values of the power-law exponent. Noted that curves represented by $n = 0$, equal to fully isotropic aluminum beam. Tension and compression stress values are not equal and affected by n. Therefore, stress distributions for FG beams differ from conventional ones. Moreover, the neutral plane position is affected too. Fig. 9 is highly deviated due to the TBT assumption of constant shear distribution and it should equal zero on upper and lower surfaces with parabolic change through-thickness. However, it can give a superficial idea about the effect of power index changing on the shear stress distribution.

5.3.3 Natural frequencies

Dynamic convergence is checked for SS-SS Ceramic/ Metal FG beam with the following material properties $E_{Ce} = 151\text{GPa}$, $\upsilon_{Ce} = 0.3$, $\rho_{Ce} = 5000\,\text{kg/m}^3$, $E_{Me} = 70\text{GPa}$, $\upsilon_{Me} = 0.3$, $\rho_{Me} = 2780\,\text{kg/m}^3$, $L/h = 100$ and unit width, as shown in Fig. 10. First natural frequency is normalized using the formula $\bar{\omega}_i = \omega_i L^2\sqrt{\frac{I_0}{E^m h^3}}$. Also,

Table 9 Single-Walled CNT with $0.067\ nm$ effective wall thickness and polymer matrix material properties

Property	CNT	Unit	Property	CNT	Unit
E_{11}^{CNT}	5.6466	TPa	E^m	2.5	GPa
E_{22}^{CNT}	7.0800	TPa	G^m	$\frac{E^m}{2(1+\upsilon^m)}$	GPa
G_{12}^{CNT}	1.9445	TPa			
ρ^{CNT}	1400	kg/m^3	ρ^m	1150	kg/m^3
υ_{12}^{CNT}	0.175	-	υ^m	0.34	-

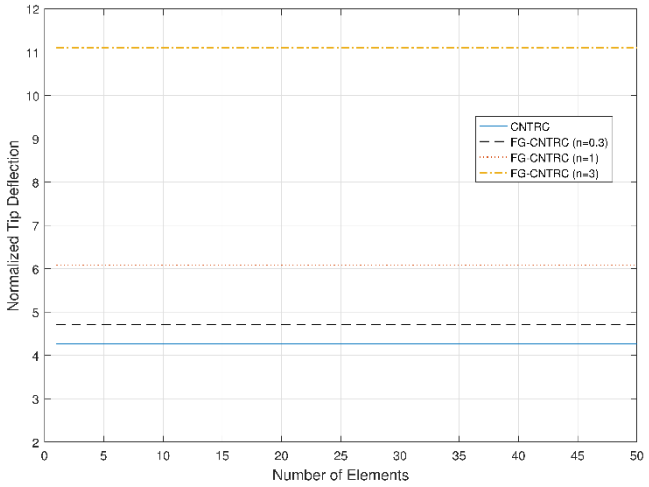

Fig. 11 Convergence of non-dimensional tip deflection for F-Free CNTRC and FG-CNTRC beams

Table 8 shows the same beam validated with an error lower than or equals 0.05% compared to (Anandrao *et al*. 2012).

5.4 CNTRC & FG-CNTRC beams

The presented model's capability is extended to cover grading index n and CNT orientation angles θ, as shown in the following results. The constituent materials are listed in Table 9 as given in Ref. Ansari *et al*. (2014), Shen and Zhang (2010).

Geometric characteristics are stated individually for each case. Final CNTRC and FG-CNTRC properties are calculated based on Eqs. (3) and (5) and efficiency parameters as Table 1.

5.4.1 Static deflection

A cantilever beam with CNT orientation angle $\theta = 0°$, $L/h = 25$, $V_{tcnt} = 0.12$ and unit width is selected to check convergence of static deflection for CNTRC and FG-CNTRC beams, as shown in Fig. 11. The superb convergence property is shown for CNTRC and FG-CNTRC beams with different n values. Non-dimensional tip displacements are obtained as $\bar{w} = \left(wAE^m h^2 10^2 / f_t L^4\right)$, and the beam is subjected to unit distributed load.

Next, normalized transverse deflection of CNTRC and FG-CNTRC beams is studied in Table 10. It is subjected to unit distributed load with different boundary conditions, power exponent n and orientation angle θ, where all deformations are calculated at $x = 0$. The normalized deflection increases

Table 10 Normalized transverse deflection of CNTRC and FG-CNTRC beams due to applied unit distributed load with different boundary conditions and orientation angle ($L/h = 25$, $x = 0$ and $V_{tcnt} = 0.12$)

B.C	θ	CNTRC	FG-CNTRC			
			$n = 0.3$	$n = 0.5$	$n = 1$	$n = 2$
F-F	0°	0.1614	0.1707	0.1780	0.1989	0.2478
	45°	2.6576	2.6895	2.7068	2.7463	2.7759
	90°	2.7701	2.7875	2.7852	2.7562	2.6607
F-SS	0°	0.2576	0.2763	0.2911	0.3332	0.4320
	45°	5.3132	5.3770	5.4115	5.4905	5.5497
	90°	5.4758	5.5107	5.5063	5.4485	5.2581
SS-SS	0°	0.4902	0.5370	0.5739	0.6797	0.9277
	45°	13.2782	13.4375	13.5238	13.7214	13.8694
	90°	13.5338	13.6210	13.6102	13.4663	12.9921
F-Free	0°	1.6351	1.7941	1.9196	2.2794	3.1231
	45°	45.1447	45.6865	45.9799	46.6519	47.1549
	90°	45.9833	46.2798	46.2430	45.7541	44.1420

Table 11 CNT and polymer matrix material properties as Yas and Samadi (2012), Wattanasakulpong and Ungbhakorn (2013)

Property	CNT	Unit	Property	CNT	Unit
E_{11}^{CNT}	600	GPa	E^m	2.5	GPa
E_{22}^{CNT}	10	GPa	G^m	$\frac{E^m}{2(1+\upsilon^m)}$	GPa
G_{12}^{CNT}	17.2	GPa			
ρ^{CNT}	1400	kg/m^3	ρ^m	1190	kg/m^3
υ_{12}^{CNT}	0.19	-	υ^m	0.3	-

Table 12 Comparisons of the non-dimensional transverse deflection of SS-SS CNTRC beam with various V_{tcnt}, $x = 0$ and $\theta = 0°$

V_{tcnt}	L/h	Unified Model	CNTRC	
			HOSDT (Wattanasakulpong and Ungbhakorn 2013)	TBT (Kumar and Srinivas 2017)
0.12	10	0.7075	0.7040	0.7037
	15	0.5255	0.5240	0.5217
	20	0.4618	0.4610	0.4580
0.17	10	0.4512	0.4490	0.4485
	15	0.3448	0.3440	0.3421
	20	0.3076	0.3070	0.3049
0.28	10	0.3270	0.3250	0.3254
	15	0.2353	0.2350	0.2337
	20	0.2032	0.2030	0.2016

in all cases from F-F, F-SS, SS-SS and F-Free, respectively. It enlarges with CNT angle increment with a considerable rise between $\theta = 0°$and $\theta = 45°$. For FG-CNTRC beams, the growth of $n$depends on each separate case with a specific boundary condition and θ.

Table 13 Comparisons of the first three dimensionless natural frequencies of SS-SS CNTRC and FG-CNTRC beams with various V_{tcnt}, $L/h = 25$ and $\theta = 0°$

V_{tcnt}	Mode No.	CNTRC Unified Model	CNTRC TBT (Ansari *et al*. 2014)	CNTRC HOSDT (Shen and Xiang 2013)	FG-CNTRC Unified Model	FG-CNTRC TBT (Ansari *et al*. 2014)	FG-CNTRC HOSDT (Shen and Xiang 2013)
0.12	1	15.8148	15.8569	15.8363	13.4511	13.4913	13.4544
	2	51.6607	51.8191	51.8139	46.1618	46.2767	46.1920
	3	93.3683	93.5513	93.8709	86.6553	86.7826	86.8513
0.17	1	19.2010	19.2565	19.2279	16.2280	16.2828	16.2286
	2	63.9514	64.1797	64.1381	56.6928	56.8608	56.6836
	3	117.2675	117.5724	117.8051	108.1098	108.3287	108.1428
0.28	1	23.4464	23.49538	23.4774	19.9925	20.0344	19.9556
	2	74.2254	74.39034	74.4687	67.3244	67.4387	66.9973
	3	131.3010	131.4391	132.2442	124.4254	124.5196	123.8009

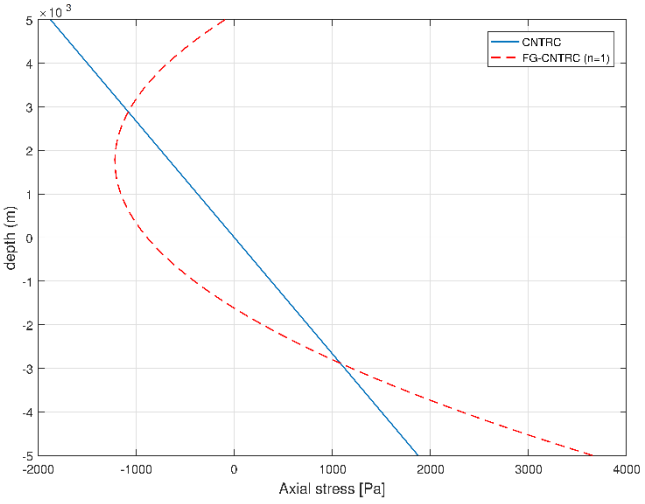

Fig. 12 Normal stress distributions for F-Free CNTRC and FG-CNTRC beams at $x = -L/2$

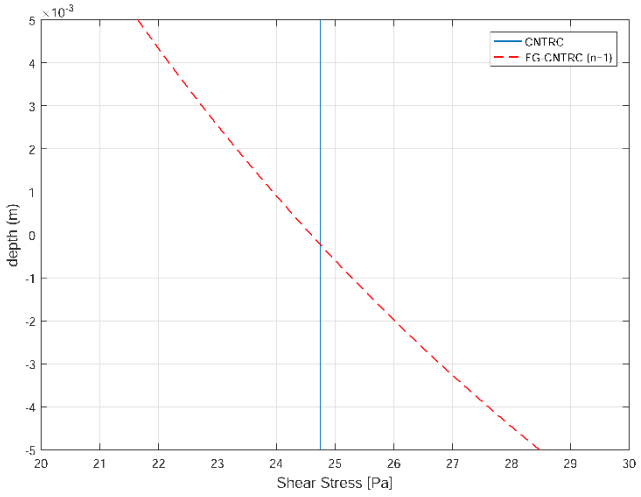

Fig. 13 Shear stress distributions for F-Free CNTRC and FG-CNTRC beams at $x = -L/2$

For validation purpose, SS-SS CNTRC beam central transverse deflection is compared to results published at (Wattanasakulpong and Ungbhakorn 2013, Kumar and Srinivas 2017), as listed in Table 12. But references parameters are changed than mentioned before and listed in Table 11. Moreover, efficiency parameters are changed to $\eta_1 = 1.2833$, $\eta_2 = \eta_3 = 1.0556$, for $V_{tcnt} = 0.12$, $\eta_1 = 1.3414$, $\eta_2 = \eta_3 = 1.7101$, for $V_{tcnt} = 0.17$ and $\eta_1 = 1.3238$, $\eta_2 = \eta_3 = 1.7380$, for $V_{tcnt} = 0.28$ as Ref. Yas and Samadi (2012), Wattanasakulpong and Ungbhakorn (2013). It also assumes that $\upsilon_{12}^{CNT} = \upsilon_{21}^{CNT} = \upsilon^{CNT}$ and normalization is done according to $\bar{w} = (wE^m h^3 10^2 / f_t L^4)$. Table 12 shows an acceptable agreement of the unified model to the published results with error less than 0.6% compared to HOSDT (Wattanasakulpong and Ungbhakorn 2013). It also shows that V_{tcnt} and L/h rise caused decrement on the transverse deflection for CNTRC beams.

5.4.2 Stress analysis

Material properties listed in Table 9 are used to investigate the stress distribution of cantilever CNTRC and FG-CNTRC beams. The beam properties are $L/h = 25$, $\theta = 0°$, $f_t = 1$ N/m, $V_{tcnt} = 0.12$ and its corresponding efficiency parameters are chosen as Table 1. Fig. 12 illustrates normal stress distribution for CNTRC beam and FG-CNTRC beam with power exponent $n = 1$. The CNTRC beam obtained traditional axial stress distribution. However, the effect of gradation appeared on the FG-CNTRC beam with different max-min values, cubic shape and neutral plan position. At the same time, Fig. 13 represents the constant shear stress assumption for CNTRC beams. Notwithstanding, the FG-CNTRC beam produced a non-constant shape. The exact real shape cannot be deduced properly due to TBT's weakness in shear stress representation.

5.4.3 Natural frequencies

Free-vibration analysis is performed for the first three normalized natural frequencies and compared with results published in (Shen and Xiang 2013, Ansari *et al*. 2014). The SS-SS beam material properties are listed in Table 1, 9 and normalized by $\bar{\omega}_i = \omega_i \frac{L^2}{h}\sqrt{\frac{\rho^m}{E^m}}$. Table 13 shows good agreement with the literature where error does not exceed 0.7% compared to HOSDT (Shen and Xiang 2013).

Table 14 Effect of θ and n on the first non-dimensional frequencies of CNTRC and FG-CNTRC beams with different boundary conditions $L/h = 25$ and $V_{tcnt} = 0.12$

B.C.	θ	CNTRC	FG-CNTRC			
			$n = 0.3$	$n = 0.5$	$n = 1$	$n = 2$
F-F	0°	1.0437	1.0162	0.9956	0.9429	0.846
	45°	0.2592	0.2583	0.2575	0.2556	0.2543
	90°	0.2538	0.2536	0.2537	0.2551	0.2596
F-SS	0°	0.8174	0.7899	0.7695	0.7187	0.6306
	45°	0.1787	0.1781	0.1775	0.1762	0.1753
	90°	0.1761	0.176	0.176	0.177	0.1801
SS-SS	0°	0.5949	0.5693	0.5507	0.506	0.433
	45°	0.1145	0.114	0.1137	0.1128	0.1122
	90°	0.1134	0.1132	0.1133	0.1139	0.1159
F-Free	0°	0.222	0.2114	0.204	0.1863	0.1581
	45°	0.0408	0.0406	0.0405	0.0402	0.04
	90°	0.0405	0.0404	0.0404	0.0406	0.0414

Moreover, Table 14 presents first non-dimensional natural frequency for CNTRC and FGCNTRC with different boundary conditions, θ and n. The normalization is conducted according to $\bar{\omega}_i = \omega_i L\sqrt{\frac{I_0^m}{A_{11}^m}}$ where, $I_0^m = \int_A \rho^m . dA$ is the first mass coefficient for homogeneous polymer matrix beam and $A_{11}^m = \int_A E^m . dA$ is the first stiffness coefficient for homogeneous polymer matrix beam.

6. Conclusions

This article proposes a unified shape function for modeling and analyzing of isotropic, orthotropic, FGM, nanocomposite and FG nanocomposite beams. Theoretical and FE derivations are presented based on TBT and two-nodes element with six degrees of freedom. Furthermore, the static analysis validations prove the model accuracy and super-convergence property where static results can be obtained using only one element. This property reduces computational time and, in turn, cost. Moreover, the element satisfies the patch test because it is proved to be monotonic convergence, conforming and satisfied both completeness and compatibility conditions. The stress analysis results are acceptable on normal stress behavior. However, it suffers from error due to constant shear stress assumptions on TBT in shear investigations, whereas upper and lower surface shear stress values must be equal to zero. Also, natural frequencies are studied and showed high-accuracy in comparison with published results. Outcomes can be summarized as follows.

• Unified shape function depends on material properties and cross-section geometry.

• The model can overcome the FE problems by analyzing continuously changed materials properties such as FGM and FG-CNTRC.

• The model is convergent, free-off shear locking, suitable for short or long beams and generalized for selected advanced materials.

• For CNTRC and FG-CNTRC, the model abilities extend to cover CNT orientation angle and power-law exponent with acceptable precision.

• The proposed approach improves the old-concept of FE modeling and it presented a solution for advanced material modeling.

• The proposed enhancements could be extended to help develop new software features to cope with the rapid progress of structural materials.

The future work will include extensible of the presented approach to more complicated shapes such as plates and shells.

References

Anandrao, K.S., Gupta, R.K., Ramachandran, P. and Rao, G.V. (2012), "Free vibration analysis of functionally graded beams", *Defence Sci. J.*, **62**(3), 139-146, https://doi.org/10.14429/dsj.62.1326.

Ansari, R., Shojaei, M.F., Mohammadi, V., Gholami, R. and Sadeghi, F. (2014), "Nonlinear forced vibration analysis of functionally graded carbon nanotube-reinforced composite timoshenko beams", *Compos. Struct.*, **113**, 316-327, https://doi.org/10.1016/j.compstruct.2014.03.015.

Aydogdu, M. (2014), "On the vibration of aligned carbon nanotube reinforced composite beams", *Adv. Nano Res.*, **2**(4), 199-210. http://doi.org/10.12989/anr.2014.2.4.199.

Baiges, J., Codina, R., Castañar, I. and Castillo, E. (2020), "A finite element reduced-order model based on adaptive mesh refinement and artificial neural networks", *Int. J. Numer. Meth. Eng.*, **121**(4), 588-601, https://doi.org/10.1002/nme.6235.

Barati, M.R. and Shahverdi, H. (2020), "Finite element forced vibration analysis of refined shear deformable nanocomposite graphene platelet-reinforced beams", *J. Brazil. Soc. Mech. Sci. Eng.*, **42**(1), 33, https://doi.org/10.1007/s40430-019-2118-8.

Bazoune, A., Khulief, Y. and Stephen, N. (2003), "Shape functions of three-dimensional Timoshenko beam element", *J. Sound Vib.*, **259**(2), 473-480, https://doi.org/10.1006/jsvi.2002.5122.

Berghouti, H., Adda Bedia, E., Benkhedda, A. and Tounsi, A. (2019), "Vibration analysis of nonlocal porous nanobeams made of functionally graded material", *Adv. Nano Res.*, **7**(5), 351-364, https://doi.org/10.12989/ANR.2019.7.5.351.

Bogue, R. (2014), "Smart materials: A review of capabilities and applications", *Assembly Auto.*, **34**(3). https://doi.org/10.1108/AA-10-2013-094.

Caraballo, S. (2011), "Thermo-mechanical beam element for analyzing stresses in functionally graded materials", Ph.D. Thesis, University of South Florida, Florida, U.S.A.

Chakraborty, A., Gopalakrishnan, S. and Reddy, J. (2003), "A new beam finite element for the analysis of functionally graded materials", *Int. J. Mech. Sci.*, **45**(3), 519-539. https://doi.org/10.1016/S0020-7403(03)00058-4.

Chakraborty, A., Mahapatra, D.R. and Gopalakrishnan, S. (2002), "Finite element analysis of free vibration and wave propagation in asymmetric composite beams with structural discontinuities", *Compos. Struct.*, **55**(1), 23-36. https://doi.org/10.1016/S0263-8223(01)00130-1.

Chandrashekhara, K. and Bangera, K.M. (1992), "Free vibration of composite beams using a refined shear flexible beam element", *Comput. Struct.*, **43**(4), 719-727. https://doi.org/10.1016/0045-7949(92)90514-Z.

Chandrashekhara, K., Krishnamurthy, K. and Roy, S. (1990), "Free vibration of composite beams including rotary inertia and shear deformation", *Compos. Struct.*, **14**(4), 269-279. https://doi.org/10.1016/0263-8223(90)90010-C.

Cook, R.D. (2007), *Concepts and Applications of Finite Element Analysis*, John wiley & sons.

Dabbagh, A., Rastgoo, A. and Ebrahimi, F. (2020), "Post-buckling analysis of imperfect multi-scale hybrid nanocomposite beams rested on a nonlinear stiff substrate", *Eng. Comput.*, 1-14. ttps://doi.org/10.1007/s00366-020-01064-1.

Dabbagh, A., Rastgoo, A. and Ebrahimi, F. (2021), "Thermal buckling analysis of agglomerated multiscale hybrid nanocomposites via a refined beam theory", *Mech. Based Des. Struct.*, **49**(3), 403-429. https://doi.org/10.1080/15397734.2019.1692666.

Ebrahimi, F. and Dabbagh, A. (2018a), "Effect of humid-thermal environment on wave dispersion characteristics of single-layered graphene sheets", *Appl. Phys. A*, **124**(4), 1-11. https://doi.org/10.1007/s00339-018-1734-y.

Ebrahimi, F. and Dabbagh, A. (2018b), "On wave dispersion characteristics of double-layered graphene sheets in thermal environments", *J. Electromagnet. Waves.*, **32**(15), 1869-1888. https://doi.org/10.1080/09205071.2017.1417918.

Ebrahimi, F. and Dabbagh, A. (2018c), "Wave dispersion characteristics of embedded graphene platelets-reinforced composite microplates", *Eur. Phys. J. Plus*, **133**(4), 1-13. https://doi.org/10.1140/epjp/i2018-11956-5.

Ebrahimi, F. and Dabbagh, A. (2019a), "Application of the nonlocal strain gradient elasticity on the wave dispersion behaviors of inhomogeneous nanosize beams", *Eur. Phys. J. Plus*, **134**(3), 112. https://doi.org/10.1140/epjp/i2019-12464-x.

Ebrahimi, F. and Dabbagh, A. (2019b), "Vibration analysis of graphene oxide powder-/carbon fiber-reinforced multi-scale porous nanocomposite beams: A finite-element study", *Eur. Phys. J. Plus*, **134**(5), 1-15. https://doi.org/10.1140/epjp/i2019-12594-1.

Ebrahimi, F. and Dabbagh, A. (2019c), "Wave dispersion characteristics of heterogeneous nanoscale beams via a novel porosity-based homogenization scheme", *Eur. Phys. J. Plus*, **134**(4), 1-8. https://doi.org/10.1140/epjp/i2019-12510-9.

Ebrahimi, F. and Dabbagh, A. (2019d), *Wave Propagation Analysis of Smart Nanostructures, CRC Press.* https://doi.org/10.1201/9780429279225.

Ebrahimi, F. and Dabbagh, A. (2020a), "A brief review on the influences of nanotubes' entanglement and waviness on the mechanical behaviors of cntr polymer nanocomposites", *J. Comput. Appl. Mech.*, **51**(1), 247-252. https://doi.org/10.22059/jcamech.2020.304476.517.

Ebrahimi, F. and Dabbagh, A. (2020b), *Mechanics of Nanocomposites: Homogenization and Analysis*, CRC Press. https://doi.org/10.1201/9780429316791.

Ebrahimi, F. and Dabbagh, A. (2020c), "Vibration analysis of multi-scale hybrid nanocomposite shells by considering nanofillers' aggregation", *Waves Random Complex Med.*, 1-19. https://doi.org/10.1080/17455030.2020.1810363.

Ebrahimi, F. and Dabbagh, A. (2020d), "Viscoelastic wave propagation analysis of axially motivated double layered graphene sheets via nonlocal strain gradient theory", *Waves Random Complex Med.*, **30**(1), 157-176. https://doi.org/10.1080/17455030.2018.1490505.

Ebrahimi, F. and Dabbagh, A. (2021), "An analytical solution for static stability of multiscale hybrid nanocomposite plates", *Eng. Comput.*, **37**(1), 545-559. https://doi.org/10.1007/s00366-019-00840-y.

Ebrahimi, F., Dabbagh, A., Rabczuk, T. and Tornabene, F. (2019a), "Analysis of propagation characteristics of elastic waves in heterogeneous nanobeams employing a new two-step porosity-dependent homogenization scheme", *Adv. Nano Res.*, **7**(2), 135-143. https://doi.org/10.12989/anr.2019.7.2.135.

Ebrahimi, F., Dabbagh, A. and Rastgoo, A. (2019b), "Vibration analysis of porous metal foam shells rested on an elastic substrate", *J. Strain Anal. Eng.*, **54**(3), 199-208. https://doi.org/10.1177/0309324719852555.

Ebrahimi, F., Dabbagh, A. and Rastgoo, A. (2020), "Static stability analysis of multi-scale hybrid agglomerated nanocomposite shells", *Mech. Based Des. Struct.*, 1-17. https://doi.org/10.1080/15397734.2020.1848585.

Ebrahimi, F., Dabbagh, A. and Rastgoo, A. (2021a), "Free vibration analysis of multi-scale hybrid nanocomposite plates with agglomerated nanoparticles", *Mech. Based Des. Struct.*, **49**(4), 487-510. https://doi.org/10.1080/15397734.2019.1692665.

Ebrahimi, F., Dabbagh, A. and Taheri, M. (2021b), "Vibration analysis of porous metal foam plates rested on viscoelastic substrate", *Eng. Comput.*, **37**(4), 3727-3739. https://doi.org/10.1007/s00366-020-01031-w.

Ebrahimi, F. and Habibi, S. (2017), "Low-velocity impact response of laminated fg-cnt reinforced composite plates in thermal environment", *Adv. Nano Res.*, **5**(2), 69-97. http://doi.org/10.12989/anr.2017.5.2.069.

Ebrahimi, F., Haghi, P. and Dabbagh, A. (2018), "Analytical wave dispersion modeling in advanced piezoelectric double-layered nanobeam systems", *Struct. Eng. Mech., Int. J*, **67**(2), 175-183. https://doi.org/10.12989/sem.2018.67.2.175.

Ebrahimi, F., Khosravi, K. and Dabbagh, A. (2021c), "Wave dispersion in viscoelastic fg nanobeams via a novel spatial-temporal nonlocal strain gradient framework", *Waves Random Complex Med.*, pages 1-23. https://doi.org/10.1080/17455030.2021.1970282.

Ebrahimi, F., Nopour, R. and Dabbagh, A. (2021d), "Effect of viscoelastic properties of polymer and wavy shape of the cnts on the vibrational behaviors of cnt/glass fiber/polymer plates", *Eng. Comput.*, 1-14. https://doi.org/10.1007/s00366-021-01387-7.

Ebrahimi, F., Seyfi, A. and Dabbagh, A. (2019c), "Dispersion of waves in fg porous nanoscale plates based on nsgt in thermal environment", *Adv. Nano Res.*, **7**(5), 325-335. https://doi.org/10.12989/anr.2019.7.5.325.

Ebrahimi, F., Seyfi, A. and Dabbagh, A. (2019d), "A novel porosity-dependent homogenization procedure for wave dispersion in nonlocal strain gradient inhomogeneous nanobeams", *Eur. Phys. J. Plus*, **134**(5), 1-11. https://doi.org/10.1140/epjp/i2019-12547-8.

Ebrahimi, F., Seyfi, A. and Dabbagh, A. (2021e), "The effects of thermal loadings on wave propagation analysis of multi-scale hybrid composite beams", *Waves Random Complex Med.*, 1-24. https://doi.org/10.1080/17455030.2021.1956015.

Eisenberger, M. (1994), "Derivation of shape functions for an exact 4-dof timoshenko beam element", *Commun. Numer. Meth. Eng.*, **10**(9), 673-681. https://doi.org/10.1002/cnm.1640100902.

Eisenberger, M. (2003), "An exact high order beam element", *Comput. Struct.*, **81**(3), 147-152. https://doi.org/10.1016/S0045-7949(02)00438-8.

El-Ashmawy, A., Kamel, M. and Elshafei, M. (2016a), "A generalized non-conventional finite element model for analysis of isotropic, orthotropic and function graded beams", *ERJ-Faculty Eng. Shoubra*, **28**(5), 63-83.

El-Ashmawy, A., Kamel, M. and Elshafei, M.A. (2016b), "Thermo-mechanical analysis of axially and transversally function graded beam", *Compos. Part B Eng.*, **102**, 134-149. https://doi.org/10.1016/j.compositesb.2016.07.015.

El-Ashmawy, A. and Xu, Y. (2020), "Longitudinal modeling and properties tailoring of functionally graded carbon nanotube

reinforced composite beams: A novel approach", *Appl. Math. Modell.*, **88**, 161-174. https://doi.org/10.1016/j.apm.2020.06.043.

El-Ashmawy, A., Xu, Y. and Aziz, L. (2021), "Mechanical properties improvement of bidirectional functionally graded laminated mwcnt reinforced composite beams using an integrated tailoring-optimization approach", *Micropor. Mesopor. Mater.*, **314**, 110875. https://doi.org/10.1016/j.micromeso.2021.110875.

El-Ashmawy, A.M. and Xu, Y. (2021), "Combined effect of carbon nanotubes distribution and orientation on functionally graded nanocomposite beams using finite element analysis", *Mater. Res. Exp.*, **8**(1), 015012. https://doi.org/10.1088/2053-1591/abc773.

Elshafei, M.A. (2013), "Fe modeling and analysis of isotropic and orthotropic beams using first order shear deformation theory", *Mater. Sci. Appl.*, **4**(1), 26. https://doi.org/10.4236/msa.2013.41010.

Emdadi, M., Mohammadimehr, M. and Navi, B.R. (2019), "Free vibration of an annular sandwich plate with cntrc facesheets and fg porous cores using ritz method", *Adv. Nano Res.*, **7**(2), 109-123. http://doi.org/10.12989/anr.2019.7.2.109.

Farzad Ebrahimi, Ali Dabbagh, A.R.T.R. (2020), "Agglomeration effects on static stability analysis of multiscale hybrid nanocomposite plates", *Comput. Mater. Continua*, **63**(1), 41-64. https://doi.org/10.32604/cmc.2020.07947.

Feng, D.C. and Wu, J.Y. (2020), "Improved displacement-based timoshenko beam element with enhanced strains", *J. Struct. Eng.*, **146**(3), 04019221. https://doi.org/10.1061/(ASCE)ST.1943-541X.0002549.

Filippi, M., Carrera, E. and Zenkour, A. (2015), "Static analyses of fgm beams by various theories and finite elements", *Compos. Part B Eng.*, **72**, 1-9. https://doi.org/10.1016/j.compositesb.2014.12.004.

Friedman, Z. and Kosmatka, J. B. (1993), "An improved two-node timoshenko beam finite element", *Comput. Struct.*, **47**(3), 473-481. https://doi.org/10.1016/0045- 949(93)90243-7.

Frikha, A., Hajlaoui, A., Wali, M. and Dammak, F. (2016), "A new higher order c0 mixed beam element for fgm beams analysis", *Compos. Part B Eng.*, **106**, 181-189. https://doi.org/10.1016/j.compositesb.2016.09.024.

Gibson, R.F. (2016), *Principles of Composite Material Mechanics*, CRC press.

Han, Y. and Elliott, J. (2007), "Molecular dynamics simulations of the elastic properties of polymer/carbon nanotube composites", *Comput. Mater. Sci.*, **39**(2), 315-323. https://doi.org/10.1016/j.commatsci.2006.06.011.

Haskul, M. (2020), "Elastic state of functionally graded curved beam on the plane stress state subject to thermal load", *Mech. Based Des. Struct.*, **48**(6), 739-754. https://doi.org/10.1080/15397734.2019.1660890.

Heshmati, M. and Yas, M. (2013), "Free vibration analysis of functionally graded cnt-reinforced nanocomposite beam using eshelby-mori-tanaka approach", *J. Mech. Sci. Technol.*, **27**(11), 3403-3408. https://doi.org/10.1007/s12206-013-0862-8.

Hocaoğlu, M. and Karagülle, H. (2020), "Effect of carbon nanotube reinforcement on the natural frequencies and damping ratios of nanocomposite beams", *Mater. Res. Express*, **7**(2), 25021. https://doi.org/10.1088/2053-1591/ab721a.

Hou, H. and He, G. (2018), "Static and dynamic analysis of two-layer timoshenko composite beams by weak-form quadrature element method", *Appl. Math. Modell.*, **55**, 466-483. https://doi.org/10.1016/j.apm.2017.11.007.

Huang, Y. and Ouyang, Z.Y. (2020), "Exact solution for bending analysis of two-directional functionally graded timoshenko beams", *Arch. Appl. Mech.*, 1-19. https://doi.org/10.1007/s00419-019-01655-5.

Iwai, R. and Kobayashi, N. (2003), "A new flexible multibody beam element based on the absolute nodal coordinate formulation using the global shape function and the analytical mode shape function", *Nonlinear Dyn.*, **34**(1-2), 207-232. https://doi.org/10.1023/B:NODY.0000014560.78333.76.

Katili, I., Syahril, T. and Katili, A.M. (2020), "Static and free vibration analysis of fgm beam based on unified and integrated of timoshenko's theory", *Compos. Struct.*, 112130. https://doi.org/10.1016/j.compstruct.2020.112130.

Ke, L.L., Yang, J. and Kitipornchai, S. (2013), "Dynamic stability of functionally graded carbon nanotube reinforced composite beams", *Mech. Adv. Mater. Struct.*, **20**(1), 28-37. https://doi.org/10.1080/15376494.2011.581412.

Kennedy, G.J., Hansen, J.S. and Martins, J.R. (2011), "A timoshenko beam theory with pressure corrections for layered orthotropic beams", *Int. J. Solid Struct.*, **48**(16-17), 2373-2382. https://doi.org/10.1016/j.ijsolstr.2011.04.009.

Khan, M.A., Yasin, M., Beg, M.S. and Khan, A. (2020), "Free and forced vibration analysis of functionally graded beams using finite element model based on refined third-order theory", *Emerging Trends Mech. Engi.*, 603-612. https://doi.org/10.1007/978-981-32-9931-3_58.

Khdeir, A. and Reddy, J. (1997), "An exact solution for the bending of thin and thick cross-ply laminated beams", *Compos. Struct.*, **37**(2), 195-203. https://doi.org/10.1016/S0263-8223(97)80012-8.

Kocatürk, T. and Şimşek, M. (2005), "Free vibration analysis of timoshenko beams under various boundary conditions", *Sigma*, **1**, 30-44.

Kumar, P. and Srinivas, J. (2017), "Free vibration, bending and buckling of a fg-cnt reinforced composite beam", *Multidiscip. Model. Mater. Struct.*, **13**(4), 590-611. https://doi.org/10.1108/MMMS-05-2017-0032.

Lee, J. and Schultz, W. (2004), "Eigenvalue analysis of timoshenko beams and axisymmetric mindlin plates by the pseudospectral method", *J. Sound Vib.*, **269**(3-5), 609-621. https://doi.org/10.1016/S0022- 0X(03)00047-6.

Lees, A. and Thomas, D. (1982), "Unified timoshenko beam finite element", *J. Sound Vib.*, **80**(3), 355-366. https://doi.org/10.1016/0022-460X(82)90276-0.

Lezgy-Nazargah, M. (2020), "A four-variable global-local shear deformation theory for the analysis of deep curved laminated composite beams", *Acta Mechanica*, pages 1-32. https://doi.org/10.1007/s00707-019-02593-7.

Li, N., Huang, S., Zhang, G., Qin, R., Liu, W., Xiong, H., Shi, G. and Blackburn, J. (2019), "Progress in additive manufacturing on new materials: A review", *J. Mater. Sci. Technol.*, **35**(2), 242-269. https://doi.org/10.1016/j.jmst.2018.09.002.

Li, N., Li, Z. and Xie, L. (2013), "A fiber-section model based timoshenko beam element using shear-bending interdependent shape function", *Earthq. Eng. Eng. Vib.*, **12**(3), 421-432. https://doi.org/10.1007/s11803-013-0183-z.

Li, W. and Han, B. (2018), "Research and application of functionally gradient materials", *IOP Conference Series Mater. Sci. Eng.*, **22065**. https://doi.org/10.1088/1757-899X/394/2/022065.

Li, X.F. (2008), "A unified approach for analyzing static and dynamic behaviors of functionally graded timoshenko and euler-bernoulli beams", *J. Sound Vib.*, **318**(4-5), 1210-1229. https://doi.org/10.1016/j.jsv.2008.04.056.

Liu, H., Wu, H. and Lyu, Z. (2020), "Nonlinear resonance of fg multilayer beam-type nanocomposites: Effects of graphene nanoplatelet-reinforcement and geometric imperfection", *Aerosp. Sci. Technol.*, **98**, 105702. https://doi.org/10.1016/j.ast.2020.105702.

Mansouri, L., Arezki, D., Khatir, S., Behtani, A., Tiachacht, S., Slimani, M. and Wahab, M.A. (2020), "A comparative study of

the behavior of glass fiber-reinforced polyester composite laminates under static loading", *Proceedings of the 13th International Conference on Damage Assessment of Structures*, 875-886. https://doi.org/10.1007/978-981-13-8331-1_70.

Minghini, F., Tullini, N. and Laudiero, F. (2007), "Locking-free finite elements for shear deformable orthotropic thin-walled beams", *Int. J. Numer. Meth. Eng.*, **72**(7), 808-834. https://doi.org/10.1002/nme.2034.

Mojiri, H. and Salami, S. J. (2020), "Free vibration and dynamic transient response of functionally graded composite beams reinforced with graphene nanoplatelets (gpls) resting on elastic foundation in thermal environment", *Mech. Based Des. Struct.*, 1-21. https://doi.org/10.1080/15397734.2020.1766492.

Nabi, S. M. and Ganesan, N. (1994), "A generalized element for the free vibration analysis of composite beams", *Comput. Struct.*, **51**(5), 607-610. https://doi.org/10.1016/0045-7949(94)90068-X.

Panchore, V., Ganguli, R. and Omkar, S. (2015), "Meshless local petrov-galerkin method for rotating timoshenko beam: A locking-free shape function formulation", *Comput. Model. Eng. Sci.*, **108**(4), 215-237.

Ping, L. (2005), "Generation of hermitian shape functions for straight beam element using constructing function method", *J. Struct. Eng.*, **31**(4), 243-248.

Rajasekaran, S. and Khaniki, H.B. (2018), "Free vibration analysis of bi-directional functionally graded single/multi-cracked beams", *Int. J. Mech. Sci.*, **144**, 341-356. https://doi.org/10.1016/j.ijmecsci.2018.06.004.

Ranjbar, M. and Feli, S. (2018), "Low velocity impact analysis of an axially functionally graded carbon nanotube reinforced cantilever beam", *Polym. Compos.*, **39**(S2), E969-E983. https://doi.org/10.1002/pc.24386.

Reddy, J. (1997), "On locking-free shear deformable beam finite elements", *Comput. Meth. Appl. Mech. Eng.*, **149**(1-4), 113-132. https://doi.org/10.1016/S0045-7825(97)00075-3.

Reddy, J. and Chin, C. (1998), "Thermomechanical analysis of functionally graded cylinders and plates", *J. Therm. Stress.*, **21**(6), 593-626. https://doi.org/10.1080/01495739808956165.

Reddy, J.N. (2003), *Mechanics of Laminated Composite Plates and Shells: Theory and Analysis*, CRC press.

Sahin, S., Karahan, E., Kilic, B. and Ozdemir, O. (2019), "Finite element method for vibration analysis of timoshenko beams", *Proceedings in 2019 9th International Conference on Recent Advances in Space Technologies (RAST)*, 673-679. https://doi.org/10.1109/RAST.2019.8767827.

Selvaraj, R. and Ramamoorthy, M. (2020), "Experimental and finite element vibration analysis of cnt reinforced mr elastomer sandwich beam", *Mech. Based Des. Struct.*, 1-13. https://doi.org/10.1080/15397734.2020.1778487.

Sevilla, R., Fernández-Méndez, S. and Huerta, A. (2011), "Nurbs-enhanced finite element method (nefem)", *Arch. Comput. Meth. Eng.*, **18**(4), 441. https://doi.org/10.1007/s11831-011-9066-5.

Shen, H.S. (2009), "Nonlinear bending of functionally graded carbon nanotube-reinforced composite plates in thermal environments", *Compos. Struct.*, **91**(1), 9-19. https://doi.org/10.1016/j.compstruct.2009.04.026.

Shen, H.S. and Xiang, Y. (2013), "Nonlinear analysis of nanotube-reinforced composite beams resting on elastic foundations in thermal environments", *Eng. Struct.*, **56**, 698-708. https://doi.org/10.1016/j.engstruct.2013.06.002.

Shen, H.S. and Zhang, C.L. (2010), "Thermal buckling and postbuckling behavior of functionally graded carbon nanotube-reinforced composite plates", *Mater. Des.*, **31**(7), 3403-3411. https://doi.org/10.1016/j.matdes.2010.01.048.

Simsek, M. (2009), "Static analysis of a functionally graded beam under a uniformly distributed load by ritz method", *Int. J. Eng. Appl. Sci.*, **1**(3), 1-11.

Şimşek, M. and Kocatürk, T. (2007), "Free vibration analysis of beams by using a third-order shear deformation theory", *Sadhana*, **32**(3), 167-179. https://doi.org/10.1007/s12046-007-0015-9.

Sinha, G.P. and Kumar, B. (2020), "Review on vibration analysis of functionally graded material structural components with cracks", *J. Vib. Eng. Technol.*, 1-27. https://doi.org/10.1007/s42417-020-00208-3.

Soni, S.K., Thomas, B. and Kar, V.R. (2020), "A comprehensive review on cnts and cnt-reinforced composites: Syntheses, characteristics and applications", *Mater. Today Commun.*, 101546. https://doi.org/10.1016/j.mtcomm.2020.101546.

Suresh, S. and Mortensen, A. (1998), *Fundamentals of Functionally Graded Materials*, The Institute of Materials.

Takahashi, Y. (2006), "Study on the shape function of the 2-dimensional beam element formulated by absolute nodal coordinates", *Proceedings of Dynamics and Design Conference 2006 of the Japan Society of Mechanical Engineers*, **70**.

Talò, M., Carboni, B., Formica, G., Lanzara, G., Snyder, M. and Lacarbonara, W. (2020), *Nonlinear Dynamic Response of Nanocomposite Cantilever Beams*, in *New Trends in Nonlinear Dynamics*, 49-57. https://doi.org/10.1007/978-3-030-34724-6_6.

Tayeb, T.S., Zidour, M., Bensattalah, T., Heireche, H., Benahmed, A. and Bedia, E. (2020), "Mechanical buckling of fg-cnts reinforced composite plate with parabolic distribution using hamilton's energy principle", *Adv. Nano Res.*, **8**(2), 135-148. https://doi.org/10.12989/anr.2020.8.2.135.

Thostenson, E.T., Ren, Z. and Chou, T.W. (2001), "Advances in the science and technology of carbon nanotubes and their composites: A review", *Compos. Sci. Technol.*, **61**(13), 1899-1912. https://doi.org/10.1016/S0266-3538(01)00094-X.

Tudjono, S., Han, A., Nguyen, D.K., Kiryu, S. and Gan, B.S. (2017), "Exact shape functions for timoshenko beam element", *J. Comput. Eng.*, **19**(3), 12-20. https://doi.org/10.9790/0661-1903041220.

Vo-Duy, T., Ho-Huu, V. and Nguyen-Thoi, T. (2019), "Free vibration analysis of laminated fg-cnt reinforced composite beams using finite element method", *Front. Struct. Civil Eng.*, **13**(2), 324- 336. https://doi.org/10.1007/s11709-018-0466-6.

Wang, Y., Xie, K. and Fu, T. (2020), "Vibration analysis of functionally graded graphene oxide-reinforced composite beams using a new ritz-solution shape function", *J. Brazil. Soc. Mech. Sci. Eng.*, **42**(4), 1-14. https://doi.org/10.1007/s40430-020-2258-x.

Wattanasakulpong, N. and Ungbhakorn, V. (2013), "Analytical solutions for bending, buckling and vibration responses of carbon nanotube-reinforced composite beams resting on elastic foundation", *Comput. Mater. Sci.*, **71**, 201-208. https://doi.org/10.1016/j.commatsci.2013.01.028.

Wu, H., Yang, J. and Kitipornchai, S. (2016), "Nonlinear vibration of functionally graded carbon nanotubereinforced composite beams with geometric imperfections", *Compos. Part B Eng.*, **90**, 86-96. https://doi.org/10.1016/j.compositesb.2015.12.007.

Wu, Z., Zhang, Y., Yao, G. and Yang, Z. (2019), "Nonlinear primary and super-harmonic resonances of functionally graded carbon nanotube reinforced composite beams", *Int. J. Mech. Sci.*, **153**, 321-340. https://doi.org/10.1016/j.ijmecsci.2019.02.015.

Yarali, E., Farajzadeh, M.A., Noroozi, R., Dabbagh, A., Khoshgoftar, M.J. and Mirzaali, M.J. (2020), "Magnetorheological elastomer composites: Modeling and dynamic finite element analysis", *Compos. Struct.*, **254**, 112881. https://doi.org/10.1016/j.compstruct.2020.112881.

Yas, M. and Heshmati, M. (2012), "Dynamic analysis of functionally graded nanocomposite beams reinforced by randomly oriented carbon nanotube under the action of moving load", *Appl. Math. Modell.*, **36**(4), 1371-1394.

https://doi.org/10.1016/j.apm.2011.08.037.
Yas, M. and Samadi, N. (2012), "Free vibrations and buckling analysis of carbon nanotube-reinforced composite timoshenko beams on elastic foundation", *Int. J. Press. Vessels Piping*, **98**, 119-128. https://doi.org/10.1016/j.ijpvp.2012.07.012.
Zerrouki, R., Karas, A. and Zidour, M. (2020), "Critical buckling analyses of nonlinear fgcnt reinforced nano-composite beam", *Adv. Nano Res.*, **9**(3), 211-220. https://doi.org/10.12989/anr.2020.9.3.211.
Zhou, T., Chazot, J.-D., Perrey-Debain, E. and Cheng, L. (2019), "Performance of the partition of unity finite element method for the modeling of timoshenko beams", *Comput. Struct.*, **222**, 148-154. https://doi.org/10.1016/j.compstruc.2019.07.004.
Zhou, Z., Chen, M. and Xie, K. (2020), "Nurbs-based free vibration analysis of axially functionally graded tapered timoshenko curved beams", *Appl. Math. Mech.*, 1-20. https://doi.org/10.1007/s11012-013-9847-z.

AT